

at 23 °C under a hydrogen filled balloon for 2 h, then filtered over Celite, and the filter cake was washed with MeOH. Solvent was removed under reduced pressure, and the resultant residue was redissolved in *i*-PrOH, followed by addition of *tert*-butyl-[*S*-(*R,R*)]-(−)-(1-oxiranyl-2-phenylethyl)carbamate **7** (121 mg, 0.46 mmol). The mixture was allowed to stir at 65 °C for 24 h. Solvent was then removed under reduced pressure. Flash chromatography purification (2% MeOH in CHCl₃ as the eluent) yielded the (*R*)-amine **22** (93 mg, 41%) as a yellow oil. *R_f* = 0.32 (10% MeOH in CHCl₃); ¹H NMR (500 MHz, CDCl₃) δ 1.35 (s, 18H), 1.48 (s, 24H), 1.54 (s, 3H), 1.58 (s, 3H), 2.67–2.92 (m, 10), 2.95 (d, 1H, *J* = 4.1 Hz), 2.98 (d, 1H, *J* = 4.1 Hz), 3.47 (brs, 2H), 3.78 (brs, 3H), 3.89–4.02 (m, 5H), 4.61 (brs, 1H), 4.68 (brs, 1H), 7.18–7.22 (m, 6H), 7.27–7.30 (m, 4H); ¹³C NMR (125 MHz, CDCl₃) δ 22.9, 24.2, 26.6, 27.4, 28.1, 28.3, 36.4, 51.4, 56.9, 65.9, 70.7, 70.9, 79.3, 79.4, 79.6, 80.3, 93.4, 93.7, 126.2, 128.3, 129.4, 137.5, 137.7, 152.6, 155.8; LRMS-ESI (*m/z*) [*M* + Na]⁺ 516.

(*R*)-*tert*-Butyl-4-((*N*-((2*R*,3*S*)-3-(*tert*-butoxycarbonylamino)-2-hydroxy-4-phenylbutyl)-4-methoxyphenylsulfonamido)methyl)-2,2-dimethylloxazolidine-3-carboxylate **23**. To a stirred solution of amine **22** (37 mg, 0.07 mmol) in CH₂Cl₂ (4 mL) and aqueous saturated NaHCO₃ (4 mL) was added 4-methoxybenzenesulfonyl chloride (34 mg, 0.16 mmol). This reaction mixture was stirred for 12 h followed by extraction of the aqueous layer with CH₂Cl₂; the combined organic extracts were dried over anhydrous Na₂SO₄. Removal of solvent under reduced pressure followed by flash chromatography purification (30% EtOAc in hexane as the eluent) provided compound **23** (40 mg, 80%) as a white solid. *R_f* = 0.37 (40% EtOAc in hexane); ¹H NMR (500 MHz, CDCl₃) δ 1.34 (s, 9H), 1.48 (s, 9H), 1.60 (s, 6H), 2.84–2.89 (m, 1H), 2.95–3.06 (m, 2H), 3.15 (dd, 1H, *J* = 6.5, 13.0 Hz), 3.29 (d, 1H, *J* = 9.7 Hz), 3.41 (d, 1H, *J* = 15.1 Hz), 3.77 (brs, 2H), 3.85 (s, 3H), 3.90–3.94 (m, 1H), 3.99 (d, 1H, *J* = 9.0 Hz), 4.2 (brs, 1H), 4.73 (brs, 0.5H), 4.98 (brs, 0.5H), 6.95 (d, 2H, *J* = 8.0 Hz), 7.19–7.24 (m, 3H), 7.25–7.28 (m, 2H), 7.69 (d, 2H, *J* = 8.9 Hz); ¹³C NMR (125 MHz, CDCl₃) δ 24.0, 27.4, 28.2, 28.3, 36.0, 53.3, 54.0, 55.4, 55.8, 56.3, 65.6, 72.4, 79.0, 80.9, 93.9, 114.2, 126.0, 128.1, 129.3, 129.6, 129.9, 137.8, 152.8, 155.4, 162.9; LRMS-ESI (*m/z*) [*M* + Na]⁺ 686.

(*R*)-*tert*-Butyl-4-((*N*-((2*R*,3*S*)-3-(*tert*-butoxycarbonylamino)-2-hydroxy-4-phenylbutyl)-4-nitrophenylsulfonamido)methyl)-2,2-dimethylloxazolidine-3-carboxylate **24**. To a stirred solution of amine **22** (41 mg, 0.08 mmol) in CH₂Cl₂ (4 mL) and aqueous saturated NaHCO₃ (4 mL) was added 4-nitrobenzenesulfonyl chloride (37 mg, 0.16 mmol). This reaction mixture was stirred for 12 h followed by extraction of the aqueous layer with CH₂Cl₂; the combined organic extracts were dried over anhydrous Na₂SO₄. Removal of solvent under reduced pressure followed by flash chromatography purification (30% EtOAc in hexane as the eluent) provided (*R*)-nitrosulfonamide **24** (51 mg, 92%) as a white solid. *R_f* = 0.52 (40% EtOAc in hexane); ¹H NMR (500 MHz, CDCl₃) δ 1.35 (s, 18H), 1.49 (s, 24H), 1.62 (s, 6H), 3.43 (bd, 2H, *J* = 9.6 Hz), 3.55 (d, 2H, *J* = 15.1 Hz), 3.75 (brs, 4H), 3.95 (s, 4H), 4.28 (brs, 2H), 4.63 (d, 2H, *J* = 7.8 Hz), 5.16 (brs, 2H), 7.19–7.23 (m, 6H), 7.25–7.31 (m, 4H), 7.92 (d, 4H, *J* = 8.8 Hz), 8.30 (d, 4H, *J* = 8.05 Hz); ¹³C NMR (125 MHz, CDCl₃) δ 24.0, 27.3, 28.1, 28.2, 35.8, 53.7, 54.0, 55.5, 55.9, 65.6, 72.2, 79.4, 81.3, 94.1, 124.3, 126.3, 128.2, 128.4, 129.5, 137.4, 144.3, 149.9, 153.0, 155.5; LRMS-ESI (*m/z*) [*M* + Na]⁺ 701.

tert-Butyl-(2*S*,3*R*)-3-hydroxy-4-(4-methoxy-*N*-(((*R*)-2-oxooxazolidin-4-yl)methyl)phenylsulfonamido)-1-phenylbutan-2-ylcarbamate **25**. To (*R*)-toluenesulfonate **23** (32 mg, 0.05 mmol) in methanol (3 mL) was added *p*-toluenesulfonic acid monohydrate (2 mg), and the reaction mixture was allowed to stir at 23 °C. After 12 h the reaction reached maximum conversion and did not move any further. It was quenched with saturated aqueous NaHCO₃, extracted with EtOAc, washed with water and brine, and dried over Na₂SO₄. Flash chromatography purification (30–50% EtOAc in hexane) yielded 7 mg (21%) of starting material and 18 mg (58%) of the expected primary alcohol.

The above alcohol (17 mg, 0.0278 mmol), in CH₂Cl₂ (2 mL) and Et₃N (16 μL, 0.11 mmol), was cooled to −10 °C and treated with methanesulfonyl chloride (2.5 μL, 0.03 mmol). The reaction mixture was stirred at 0 °C for 2 h, followed by removal of solvent via rotavap and pump. The resulting residue was redissolved in chloroform (2 mL), treated with DIPEA (19 μL, 0.11 mmol), refluxed for 8 h, and concentrated under reduced pressure. Flash chromatography purification (1% MeOH in CHCl₃ as the eluent) afforded (*R*)-oxazolidinone **25** (12 mg, 78%) as a white solid. *R_f* = 0.33 (5% MeOH in CHCl₃); ¹H NMR (500 MHz, CDCl₃) δ 1.32 (s, 9H), 2.77 (dd, 1H, *J* = 8.4, 13.9 Hz), 2.93–3.03 (m, 3H), 3.07 (d, 1H, *J* = 14.5 Hz), 3.13 (dd, 1H, *J* = 9.3, 14.1 Hz), 3.69–3.79 (m, 2H), 3.85 (s, 3H), 3.97 (dd, 1H, *J* = 5.2, 8.3 Hz), 4.23–4.29 (m, 1H), 4.43 (t, 1H, *J* = 8.7 Hz), 6.94 (d, 2H, *J* = 8.8 Hz), 7.18–7.24 (m, 3H), 7.26–7.30 (m, 2H), 7.64 (d, 2H, *J* = 8.6 Hz); ¹³C NMR (125 MHz, CDCl₃) δ 28.1, 35.9, 52.0, 54.1, 54.6, 54.7, 55.5, 67.4, 71.9, 79.7, 114.4, 126.3, 128.4, 128.4, 129.3, 129.4, 137.5, 155.9, 159.4, 163.2; LRMS-ESI (*m/z*) [*M* + Na]⁺ 572.

tert-Butyl-(2*S*,3*R*)-4-(4-amino-*N*-(((*R*)-2-oxooxazolidin-4-yl)-methyl)phenylsulfonamido)-3-hydroxy-1-phenylbutan-2-ylcarbamate **26**. To (*R*)-nitrosulfonamide **24** (42 mg, 0.06 mmol) in methanol (4 mL) was added *p*-toluenesulfonic acid monohydrate (2 mg), and the reaction mixture was allowed to stir at 23 °C. After 36 h the reaction appeared to have moved only 75% to completion, and formation of free amines was evident on TLC. At this point, it was quenched with saturated aqueous NaHCO₃, extracted with EtOAc, washed with water and brine, and dried over Na₂SO₄. Flash chromatography purification (30–50% EtOAc in hexane) yielded 7 mg (17%) of starting material and 24 mg (55%) of the expected primary alcohol.

The above alcohol (23 mg, 0.03 mmol), in CH₂Cl₂ (3 mL) and Et₃N (20 μL, 0.14 mmol), was cooled to −10 °C and treated with methanesulfonyl chloride (53 μL, 0.04 mmol). The reaction mixture was stirred at 0 °C for 2 h, followed by removal of solvent via rotavap and pump. The resultant residue was redissolved in chloroform (3 mL), treated with DIPEA (25 μL, 0.14 mmol), and refluxed for 12 h; product crashed out of the chloroform and was found to be only slightly soluble in methanol. Solvent was removed under reduced pressure, and the crude material was treated with methanol (3 mL) and Pd/C (3 mg). The mixture was stirred at 23 °C under a H₂ filled balloon for 2 h, then filtered over Celite, and the filter cake was washed with MeOH. Removal of solvent, followed by flash chromatography purification (3% MeOH in CHCl₃ as the eluent) provided (*R*)-oxazolidinone **26** (13 mg, 68%) as a white solid. *R_f* = 0.19 (5% MeOH in CHCl₃); ¹H NMR (500 MHz, CDCl₃) δ 1.31 (s, 9H), 2.73 (dd, 1H, *J* = 8.7, 13.6 Hz), 2.88 (dd, 1H, *J* = 9.6, 14.5 Hz), 2.91–2.94 (m, 1H), 2.98 (dd, 1H, *J* = 4.2, 13.9 Hz), 3.10 (dd, 2H, *J* = 9.2, 14.0 Hz), 3.70–3.81 (m, 2H), 3.96 (dd, 1H, *J* = 5.2, 8.4 Hz), 4.21–4.24 (m, 1H), 4.40 (t, 1H, *J* = 8.7 Hz), 4.92 (d, 1H, *J* = 8.5 Hz), 6.63 (d, 2H, *J* = 8.7 Hz), 7.17–7.21 (m, 3H), 7.25–7.28 (m, 2H), 7.46 (d, 2H, *J* = 8.4 Hz); ¹³C NMR (125 MHz, CD₃OD) δ 28.1, 29.5, 35.9, 51.9, 52.0, 54.0, 54.7, 67.5, 72.1, 79.6, 113.9, 124.4, 126.3, 128.3, 129.3, 129.4, 137.6, 155.1, 156.0, 159.5; LRMS-ESI (*m/z*) [*M* + Na]⁺ 557.

tert-Butyl-(2*S*,3*R*)-3-hydroxy-4-(4-methoxy-*N*-(((*S*)-2-oxooxazolidin-4-yl)methyl)phenylsulfonamido)-1-phenylbutan-2-ylcarbamate **27**. To a solution of the (*S*)-*tert*-butyl 4-(azidomethyl)-2,2-dimethylloxazolidine-3-carboxylate *ent*-**21** (840 mg, 3.32 mmol) in MeOH (20 mL) was added Pd/C (80 mg). This mixture was stirred at 23 °C under a hydrogen filled balloon for 2 h, then filtered over Celite, and the filter cake was washed with MeOH. Solvent was removed under reduced pressure, and the resultant residue was redissolved in *i*-PrOH, followed by addition of *tert*-butyl-[*S*-(*R,R*)]-(−)-(1-oxiranyl-2-phenylethyl)carbamate **7** (218 mg, 0.83 mmol). The mixture was allowed to stir at 65 °C for 24 h. Solvent was then removed under reduced pressure. Flash chromatography purification (2% MeOH in CHCl₃ as the eluent) yielded the corresponding (*S*)-amine (**27S**) (187 mg, 46%) as an amorphous solid. *R_f* = 0.28 (10% MeOH in CHCl₃); ¹H NMR (500 MHz, CDCl₃) δ 1.35 (s, 18H), 1.48 (s, 24H), 1.54 (s, 3H), 1.58 (s, 3H), 2.64–2.91 (m, 10), 2.95–3.03 (m, 2H), 3.44 (brs, 1H), 3.50 (brs,

1H), 3.77 (brs, 3H), 3.87–4.00 (m, 5H), 4.61 (brs, 1H), 4.64 (brs, 1H), 7.18–7.22 (m, 6H), 7.27–7.30 (m, 4H); ¹³C NMR (125 MHz, CDCl₃) δ 22.9, 24.2, 26.6, 27.4, 28.1, 28.3, 36.4, 51.4, 56.7, 56.8, 65.9, 70.6, 79.3, 79.6, 80.3, 93.4, 93.7, 126.2, 126.3, 128.3, 129.3, 137.6, 137.7, 152.5, 155.8; LRMS-ESI (*m/z*) [M + Na]⁺ 576.

To a stirred solution of above *S*-amine (22S) (85 mg, 0.17 mmol) in CH₂Cl₂ (6 mL) and aqueous saturated NaHCO₃ (6 mL) was added 4-methoxybenzenesulfonyl chloride (71 mg, 0.34 mmol). This reaction mixture was stirred for 12 h followed by extraction of the aqueous layer with CH₂Cl₂; the combined organic extracts were dried over anhydrous Na₂SO₄. Removal of solvent under reduced pressure followed by flash chromatography purification (30% EtOAc in hexane as the eluent) provided (*S*)-toluenesulfonate (23S) (107 mg, 93%) as a white solid. *R*_f = 0.40 (40% EtOAc in hexane); ¹H NMR (500 MHz, CDCl₃) δ 1.34 (s, 18H), 1.46 (s, 24H), 1.58 (s, 6H), 2.82–2.87 (m, 2H), 2.96–3.13 (m, 4H), 3.18–3.24 (m, 3H), 3.32 (brs, 1H), 3.75 (brs, 1H), 3.80 (brs, 1H), 3.84 (s, 6H), 3.89–3.93 (4H), 4.07 (d, 2H, *J* = 9.2 Hz), 4.16–4.19 (m, 2H), 4.65 (brs, 1H), 4.87 (d, 1H, *J* = 7.31 Hz), 6.93–6.97 (m, 4H), 7.18–7.23 (6H), 7.26–7.28 (m, 4H), 7.64–7.71 (4H); ¹³C NMR (125 MHz, CDCl₃) δ 23.9, 27.3, 28.1, 28.2, 35.6, 52.4, 54.3, 55.2, 55.4, 56.8, 65.6, 71.8, 79.1, 80.9, 93.8, 114.2, 126.1, 128.2, 129.3, 129.4, 129.6, 137.9, 152.6, 155.6, 162.8; LRMS-ESI (*m/z*) [M + Na]⁺ 686.

To the above (*S*)-toluenesulfonate (23S) (96 mg, 0.14 mmol) in methanol (5 mL) was added *p*-toluenesulfonic acid monohydrate (4.5 mg, 0.02 mmol), and the reaction mixture was allowed to stir at 23 °C. After 8 h the reaction reached maximum conversion and did not move any further. It was quenched with saturated aqueous NaHCO₃, extracted with EtOAc, washed with water and brine, and dried over Na₂SO₄. Flash chromatography purification (30–50% EtOAc in hexane) yielded 13 mg (13%) of starting material and 59 mg (65%) of the expected primary alcohol.

The above alcohol (58 mg, 0.09 mmol), in CH₂Cl₂ (4 mL) and Et₃N (33 μL, 0.23 mmol), was cooled to –10 °C and treated with methanesulfonyl chloride (7.9 μL, 0.1 mmol). The reaction mixture was stirred at 0 °C for 2 h, followed by removal of solvent via rotavap and pump. The resultant residue was redissolved in chloroform (4 mL), treated with DIPEA (65 μL, 0.37 mmol), refluxed for 12 h, and concentrated under reduced pressure. Flash chromatography purification (2% MeOH in CHCl₃ as the eluent) afforded *S*-oxazolidinone 27 (44 mg, 85%) as a white solid. *R*_f = 0.27 (5% MeOH in CHCl₃); ¹H NMR (500 MHz, CD₃OD) δ 1.27 (s, 9H), 2.52 (dd, 1H, *J* = 10.9, 13.7 Hz), 2.67 (dd, 1H, *J* = 8.9, 14.9 Hz), 2.83 (dd, 1H, *J* = 6.1, 14.0 Hz), 3.10 (dd, 1H, *J* = 3.5, 13.8 Hz), 3.47–3.52 (m, 2H), 3.58–3.63 (m, 1H), 3.80–3.83 (m, 1H), 3.85 (s, 3H), 4.23–4.29 (m, 1H), 4.31 (dd, 1H, *J* = 4.8, 8.9 Hz), 4.47 (t, 1H, *J* = 8.6 Hz), 7.06 (d, 2H, *J* = 8.93 Hz), 7.12–7.16 (m, 1H), 7.20–7.24 (m, 4H), 7.75 (d, 2H, *J* = 8.9 Hz); ¹³C NMR (125 MHz, CD₃OD) δ 27.1, 35.6, 52.0, 54.3, 54.6, 54.7, 55.1, 68.0, 73.3, 78.5, 114.0, 125.5, 127.6, 128.9, 129.0, 129.3, 138.6, 156.5, 160.4, 163.3; LRMS-ESI (*m/z*) [M + Na]⁺ 572.

tert-Butyl-(2*S*,3*R*)-4-(4-amino-*N*-(((*S*)-2-oxooxazolidin-4-yl)-methyl)phenylsulfonamido)-3-hydroxy-1-phenylbutan-2-ylcarbamate 28. To a stirred solution of *S*-amine (22S) (87 mg, 0.17 mmol) in CH₂Cl₂ (6 mL) and aqueous saturated NaHCO₃ (6 mL) was added 4-nitrobenzenesulfonyl chloride (78 mg, 0.35 mmol). This reaction mixture was stirred for 12 h followed by extraction of the aqueous layer with CH₂Cl₂; the combined organic extracts were dried over anhydrous Na₂SO₄. Removal of solvent under reduced pressure followed by flash chromatography purification (30% EtOAc in hexane as the eluent) provided *S*-nitrosulfonamide (24S) (102 mg, 85%) as a yellow solid. *R*_f = 0.54 (40% EtOAc in hexane); ¹H NMR (500 MHz, CDCl₃) δ 1.34 (s, 18H), 1.47 (s, 24H), 1.59 (s, 6H), 2.81 (dd, 2H, *J* = 8.0, 12.9 Hz), 3.03 (bd, 2H, *J* = 9.7 Hz), 3.16–3.36 (m, 8H), 3.82 (brs, 2H), 3.91 (dd, 4H, *J* = 5.1, 8.7 Hz), 4.00 (d, 2H, *J* = 6.2 Hz), 4.20 (q, 2H, *J* = 5.6, 5.7 Hz), 4.80 (brs, 1H), 4.86 (d, 1H, *J* = 7.2 Hz), 7.20–7.24 (m, 6H), 7.27–7.30 (m, 4H), 7.88 (d, 4H, *J* = 8.4 Hz), 8.29 (d, 4H, *J* = 8.4 Hz); ¹³C NMR (125 MHz, CDCl₃) δ 23.9, 27.3, 28.1, 28.2, 35.8, 52.3, 54.5, 54.9, 56.6, 65.5, 71.6, 79.5, 81.1, 94.0, 124.2, 126.3,

128.4, 128.4, 128.5, 129.3, 137.7, 144.0, 149.9, 152.7, 155.8, 171.0; LRMS-ESI (*m/z*) [M + Na]⁺ 701.

To the above *S*-nitrosulfonamide (24S) (92 mg, 0.13 mmol) in methanol (5 mL) was added *p*-toluenesulfonic acid monohydrate (4 mg, 0.02 mmol), and the reaction mixture was allowed to stir at 23 °C. After 18 h the reaction appeared to have moved only 50% to completion, and formation of free amines was evident on TLC. At this point it was quenched with saturated aqueous NaHCO₃, extracted with EtOAc, washed with water and brine, and dried over Na₂SO₄. Flash chromatography purification (30–50% EtOAc in hexane) yielded 32 mg (35%) of starting material and 44 mg (51%) of the expected primary alcohol.

The above alcohol (43 mg, 0.06 mmol), in CH₂Cl₂ (3 mL) and Et₃N (24 μL, 0.17 mmol), was cooled to –10 °C and treated with methanesulfonyl chloride (5.5 μL, 0.07 mmol). The reaction mixture was stirred at 0 °C for 2 h, followed by removal of solvent via rotavap and pump. The resultant residue was redissolved in chloroform (2 mL), treated with DIPEA (29 μL, 0.17 mmol), and refluxed for 12 h; product crashed out of the chloroform and was found to be only slightly soluble in methanol. Solvent was removed under reduced pressure, and the crude material was treated with methanol (4 mL) and Pd/C (5 mg). The mixture was stirred at 23 °C under a hydrogen filled balloon for 3 h, then filtered over Celite, and the filter cake was washed with MeOH. Removal of solvent followed by flash chromatography purification (3% MeOH in CHCl₃ as the eluent) provided (*S*)-oxazolidinone 28 (21 mg, 58%) as a white solid. *R*_f = 0.21 (5% MeOH in CHCl₃); ¹H NMR (500 MHz, 1:1 CD₃OD/CDCl₃) δ 1.24 (s, 9H), 2.54 (d, 1H), 2.56 (dd, 1H, *J* = 8.7, 14.9 Hz), 2.70 (dd, 1H, *J* = 7.6, 14.3 Hz), 2.97 (dd, 1H, *J* = 4.0, 13.9 Hz), 3.32 (dd, 1H, *J* = 5.0, 14.3 Hz), 3.38 (dd, 1H, *J* = 3.1, 14.8 Hz), 3.64–3.70 (m, 1H), 3.78–3.83 (m, 1H), 4.05 (dd, 1H, *J* = 5.3, 8.8 Hz), 4.16–4.20 (m, 1H), 4.39 (t, 1H, *J* = 8.7 Hz), 6.59 (d, 2H, *J* = 8.7 Hz), 7.09–7.15 (m, 3H), 7.18–7.21 (m, 2H), 7.40 (d, 2H, *J* = 8.7 Hz); ¹³C NMR (125 MHz, 1:1 CD₃OD/CDCl₃) δ 31.8, 33.4, 39.4, 53.3, 56.9, 58.5, 58.8, 59.7, 71.8, 77.4, 83.3, 117.6, 127.4, 130.0, 132.0, 133.1, 133.2, 141.9, 156.0, 160.1, 164.0; LRMS-ESI (*m/z*) [M + Na]⁺ 557.

(3*R*,3*aS*,6*aR*)-Hexahydrofuro[2,3-*b*]furan-3-yl-(2*S*,3*R*)-3-hydroxy-4-(4-methoxy-*N*-(((*R*)-2-oxooxazolidin-4-yl)methyl)phenylsulfonamido)-1-phenylbutan-2-ylcarbamate 29. A solution of *S*-aminosulfone 25 (10.9 mg, 0.02 mmol) in 30% trifluoroacetic acid (in CH₂Cl₂, 2 mL) was stirred at 23 °C for 40 min, then concentrated under reduced pressure. The residue was redissolved in CH₂Cl₂ (2 mL), treated with Et₃N (30 μL, 0.21 mmol), followed by carbonate 15 (6.3 mg, 0.02 mmol), and stirred at 23 °C for 12 h. The reaction mixture was then concentrated under reduced pressure and the residue was purified by flash chromatography (3% MeOH in CHCl₃ as the eluent) to give inhibitor 29 (10 mg, 85%) as a white solid. *R*_f = 0.54 (10% MeOH in CHCl₃); ¹H NMR (500 MHz, CDCl₃) δ 1.39 (dd, 1H, *J* = 5.5, 13.1 Hz), 1.56–1.63 (m, 1H), 2.67 (dd, 1H, *J* = 10.0, 14.0 Hz), 2.85–2.90 (m, 1H), 2.95–3.01 (m, 2H), 3.10 (dd, 1H, *J* = 4.1, 14.1 Hz), 3.20 (d, 1H, *J* = 12.8 Hz), 3.28 (dd, 1H, *J* = 9.2, 14.1 Hz), 3.63–3.72 (m, 1H), 3.73 (dd, 1H, *J* = 5.2, 9.8 Hz), 3.79 (dt, 1H, *J* = 1.6, 8.2 Hz), 3.86 (s, 3H), 3.88–3.95 (m, 3H), 4.04 (dd, 1H, *J* = 5.0, 8.8 Hz), 4.25 (brs, 1H), 4.28–4.34 (m, 1H), 4.47 (t, 1H, *J* = 8.7 Hz), 4.99 (q, 1H, *J* = 5.6, 13.4 Hz), 5.38 (d, 1H, *J* = 9.8 Hz), 5.63 (d, 1H, *J* = 5.2 Hz), 6.87 (s, 1H), 6.97 (d, 2H, *J* = 8.9 Hz), 7.16–7.22 (m, 3H), 7.24–7.28 (m, 2H), 7.69 (d, 2H, *J* = 8.8 Hz); ¹³C NMR (125 MHz, CDCl₃) δ 25.8, 35.9, 45.4, 51.9, 54.1, 55.0, 55.3, 55.6, 67.6, 69.6, 71.1, 72.5, 73.4, 109.2, 114.5, 126.4, 128.4, 128.4, 129.2, 129.4, 137.5, 155.6, 159.6, 163.3; LRMS-ESI (*m/z*) [M + Na]⁺ 628.2; HRMS-ESI (*m/z*) [M + Na]⁺ calcd for C₂₈H₃₅N₃O₁₀S 628.1941, found 628.1937.

(3*R*,3*aS*,6*aR*)-Hexahydrofuro[2,3-*b*]furan-3-yl-(2*S*,3*R*)-4-(4-amino-*N*-(((*R*)-2-oxooxazolidin-4-yl)methyl)phenylsulfonamido)-3-hydroxy-1-phenylbutan-2-ylcarbamate 30. A solution of the free amine 26 (12 mg, 0.02 mmol) in 30% trifluoroacetic acid in CH₂Cl₂ (2 mL) was stirred at 23 °C for 40 min, then concentrated under reduced pressure. The residue was redissolved in CH₂Cl₂ (2 mL), treated with carbonate 15 (7.1 mg, 0.02 mmol) and Et₃N (40

μL , 0.28 mmol), and stirred at 23 °C for 12 h at 40 °C. The reaction mixture was then concentrated under reduced pressure and the residue was purified by flash chromatography (5% MeOH in CHCl_3 as the eluent) to give inhibitor **30** (11 mg, 85%) as a white solid. $R_f = 0.26$ (10% MeOH in CHCl_3); $^1\text{H NMR}$ (500 MHz, CDCl_3) δ 1.38 (dd, 1H, $J = 5.6, 13.2$ Hz), 1.54–1.63 (m, 1H), 2.61 (dd, 1H, $J = 9.5, 13.9$ Hz), 2.83–2.91 (m, 2H), 3.10 (d, 2H, $J = 13.3$ Hz), 3.18 (dd, 1H, $J = 9.6, 13.9$ Hz), 3.62–3.70 (m, 2H), 3.78–3.84 (m, 3H), 3.88 (dd, 1H, $J = 6.0, 9.8$ Hz), 3.97 (dd, 1H, $J = 5.0, 8.9$ Hz), 4.21–4.27 (m, 1H), 4.41 (t, 1H, $J = 8.7$ Hz), 4.93 (q, 1H, $J = 5.7, 13.6$ Hz), 5.60 (d, 1H, $J = 5.2$ Hz), 5.69 (d, 1H, $J = 8.8$ Hz), 6.64 (d, 2H, $J = 8.7$ Hz), 7.16–7.19 (m, 3H), 7.21–7.26 (m, 2H), 7.45 (d, 2H, $J = 8.7$ Hz); $^{13}\text{C NMR}$ (125 MHz, CDCl_3) δ 25.7, 29.5, 36.1, 45.3, 51.7, 54.1, 54.9, 55.1, 67.5, 69.5, 70.8, 71.0, 73.2, 109.2, 113.9, 123.9, 126.3, 128.3, 129.2, 129.4, 137.7, 151.4, 155.6, 159.6; LRMS-ESI (m/z) [$M + \text{Na}$] $^+$ 613.2; HRMS-ESI (m/z) [$M + \text{Na}$] $^+$ calcd for $\text{C}_{27}\text{H}_{34}\text{N}_4\text{O}_9\text{S}$ 613.1944, found 613.1939.

(3*R*,3*a*S,6*a*R)-Hexahydrofuro[2,3-*b*]furan-3-yl-(2*S*,3*R*)-3-hydroxy-4-(4-methoxy-*N*-((*S*)-2-oxooxazolidin-4-yl)methyl)phenylsulfonamido)-1-phenylbutan-2-ylcarbamate **31**. A solution of *S*-aminosulfonamide **27** (16.5 mg, 0.03 mmol) in 30% trifluoroacetic acid (in CH_2Cl_2 , 3 mL) was stirred at 23 °C for 40 min, then concentrated under reduced pressure. The residue was redissolved in CH_2Cl_2 (3 mL), treated with Et_3N (41 μL , 0.29 mmol), followed by carbonate **15** (10 mg, 0.03 mmol), and stirred at 23 °C for 12 h. The reaction mixture was then concentrated under reduced pressure and the residue was purified by flash chromatography (3% MeOH in CHCl_3 as the eluent) to give inhibitor **31** (16 mg, 90%) as a white solid. $R_f = 0.5$ (10% MeOH in CHCl_3); $^1\text{H NMR}$ (500 MHz, CDCl_3) δ 1.32 (dd, 1H, $J = 5.4, 13.2$ Hz), 1.53–1.62 (m, 1H), 2.62 (dd, 1H, $J = 11.0, 13.8$ Hz), 2.71 (dd, 1H, $J = 7.25, 14.6$ Hz), 2.84–2.89 (m, 2H), 3.10 (dd, 1H, $J = 3.6, 14.0$ Hz), 3.61–3.67 (m, 1H), 3.74–3.82 (m, 2H), 3.86 (s, 3H), 3.87 (dd, 2H, $J = 5.8, 10.1$ Hz), 3.94–3.98 (m, 1H), 4.00–4.05 (m, 2H), 4.27–4.33 (m, 1H), 4.45 (t, 1H, $J = 8.8$ Hz), 4.99 (q, 1H, $J = 5.3, 7.7$ Hz), 5.60 (d, 1H, $J = 5.3$ Hz), 5.68 (d, 1H, $J = 9.2$ Hz), 6.98 (d, 2H, $J = 8.8$ Hz), 7.15–7.20 (m, 1H), 7.22–7.27 (m, 4H), 7.69 (d, 2H, $J = 8.8$ Hz); $^{13}\text{C NMR}$ (125 MHz, CDCl_3) δ 25.7, 43.4, 45.5, 53.2, 54.6, 54.9, 55.6, 56.5, 57.5, 69.6, 71.2, 73.3, 73.5, 109.3, 114.5, 126.3, 128.3, 129.2, 129.4, 137.8, 155.9, 159.61, 163.38; LRMS-ESI (m/z) [$M + \text{Na}$] $^+$ 628.2; HRMS-ESI (m/z) [$M + \text{Na}$] $^+$ calcd for $\text{C}_{28}\text{H}_{35}\text{N}_5\text{O}_{10}\text{S}$ 628.1941, found 628.1943.

(3*R*,3*a*S,6*a*R)-Hexahydrofuro[2,3-*b*]furan-3-yl-(2*S*,3*R*)-4-(4-amino-*N*-((*S*)-2-oxooxazolidin-4-yl)methyl)phenylsulfonamido)-3-hydroxy-1-phenylbutan-2-ylcarbamate **32**. A solution of the free amine **29** (15 mg, 0.03 mmol) in 30% trifluoroacetic acid (in CH_2Cl_2 , 3 mL) was stirred at 23 °C for 40 min, then concentrated under reduced pressure. The residue was redissolved in CH_2Cl_2 (3 mL), charged with Et_3N (60 μL , 0.42 mmol), followed by carbonate **15** (8.9 mg, 0.03 mmol), and stirred at 23 °C for 12 h at 40 °C. The reaction mixture was then concentrated under reduced pressure and the residue was purified by flash chromatography (5% MeOH in CHCl_3 as the eluent) to give inhibitor **32** (13 mg, 80%) as a white solid. $R_f = 0.32$ (10% MeOH in CHCl_3); $^1\text{H NMR}$ (500 MHz, CDCl_3) δ 1.33 (dd, 1H, $J = 8.5$ Hz), 1.53–1.62 (m, 1H), 2.59 (dd, 1H, $J = 10.5, 13.9$ Hz), 2.66 (dd, 1H, $J = 7.4, 14.7$ Hz), 2.77 (dd, 1H, $J = 8.9, 14.5$ Hz), 2.82–2.89 (m, 1H), 3.10 (dd, 1H, $J = 3.4, 14.0$ Hz), 3.36 (dd, 1H, $J = 3.5, 14.3$ Hz), 3.44 (dd, 1H, $J = 4.5, 14.6$ Hz), 3.62–3.67 (m, 1H), 3.72 (dd, 1H, $J = 5.0, 9.9$ Hz), 3.77 (dt, 1H, $J = 1.8, 8.2$ Hz), 3.87 (dd, 1H, $J = 5.8, 9.9$ Hz), 3.92–3.98 (m, 2H), 3.99 (dd, 1H, $J = 5.0, 9.0$ Hz), 4.15–4.29 (m, 1H), 4.43 (t, 1H, $J = 8.8$ Hz), 4.97 (q, 1H, $J = 5.4, 13.2$ Hz), 5.60 (d, 1H, $J = 5.3$ Hz), 6.66 (d, 2H, $J = 8.7$ Hz), 7.15–7.18 (m, 1H), 7.20–7.25 (m, 4H), 7.49 (d, 2H, $J = 8.6$ Hz); $^{13}\text{C NMR}$ (125 MHz, CDCl_3) δ 25.7, 29.5, 34.7, 45.5, 53.3, 54.6, 55.0, 56.6, 67.5, 69.6, 71.1, 73.4, 109.3, 114.0, 124.2, 126.3, 128.3, 129.2, 129.4, 137.8, 151.2, 155.8, 159.6; LRMS-ESI (m/z) [$M + \text{Na}$] $^+$ 613.2; HRMS-ESI (m/z) [$M + \text{Na}$] $^+$ calcd for $\text{C}_{27}\text{H}_{34}\text{N}_4\text{O}_9\text{S}$ 613.1944, found 613.1938.

Determination of X-ray Structure of 19b-Bound HIV Protease (WT). The stabilized HIV-1 protease with the substitutions of Q7K, L33I, L63I, C67A, and C95A that reduce autoproteolysis and aggregation²⁷ was expressed and purified as described.²⁸ These mutations do not alter the inhibitor binding site, and the stabilized protease has kinetic parameters and stability indistinguishable from those of the unsubstituted enzyme.^{27,28} Inhibitor **19b** was dissolved in dimethyl sulfoxide (DMSO). Crystals were grown by the hanging drop vapor diffusion method using 1:5 molar ratio of protease (at 3.9 mg/mL) to inhibitor. The reservoir contained 0.1 M citrate phosphate buffer, pH 5.0, 0.35 M NaCl, and 4% DMSO. Crystals were mounted on a nylon loop and flash-frozen in liquid nitrogen with a cryoprotectant of 30% (v/v) glycerol. X-ray diffraction data were collected on the SER-CAT beamline of the Advanced Photon Source, Argonne National Laboratory. Diffraction data were processed using HKL2000 to 1.29 Å resolution.²⁸ Data were reduced in space group $P2_12_12$ with unit cell dimensions of $a = 58.11$ Å, $b = 86.42$ Å, $c = 45.97$ Å with one dimer in the asymmetric unit. The structure was solved by molecular replacement using the CCP4i,^{29,30} using WT/GRL0255 complex (PDB 3DJK) as a starting model.²⁶ The structure was refined using SHELX97^{31,32} and refitted manually using the molecular graphics program COOT.³³ Alternative conformations were modeled for the protease residues where observed in the electron density maps. Anisotropic atomic displacement parameters (B -factors) were refined for all atoms including solvent molecules. Hydrogen atoms were automatically added by SHELXL in the last round of the refinement. The identity of ions and other solvent molecules from the crystallization conditions was deduced from the shape and peak height of the $2F_o - F_c$ and $F_o - F_c$ electron density, the hydrogen bond interactions, and interatomic distances. The solvent molecules were one sodium ion, two chloride ions, one glycerol molecule, and 207 water (including partial occupancy sites). The final R was 14.1% for the working set, and R_{free} was 18.2% for all data between 10 and 1.29 Å resolution. The rmsd values from ideal bonds and angle distances were 0.013 and 0.031 Å, respectively. The average B -factor was 15.9 and 22.7 Å² for protease main chain and side chain atoms, respectively, 14.1 Å² for inhibitor atoms, and 32.1 Å² for water atoms. The crystallographic coordinates and structure factors have been deposited in the Protein Databank (PDB) with access code 3H5B.^{34,35}

Acknowledgment. The research was supported by grants from the National Institutes of Health (Grant GM53386 to A.K.G. and Grant GM62920 to I.T.W.). This work was also supported by the Intramural Research Program of the Center for Cancer Research, National Cancer Institute, National Institutes of Health, and in part by a Grant-in-aid for Scientific Research (Priority Areas) from the Ministry of Education, Culture, Sports, Science, and Technology of Japan (Monbu Kagakusho), a Grant for Promotion of AIDS Research from the Ministry of Health, Welfare, and Labor of Japan (Kosei Rohdoshu, Grant H15-AIDS-001), and the Grant to the Cooperative Research Project on Clinical and Epidemiological Studies of Emerging and Reemerging Infectious Diseases (Renkei Jigyo, No. 78, Kumamoto University) of Monbu-Kagakusho. We thank the staff at the SER-CAT beamline at the Advanced Photon Source, Argonne National Laboratory, for assistance during X-ray data collection. Use of the Advanced Photon Source was supported by the U.S. Department of Energy, Office of Science, Office of Basic Energy Sciences, under Contract No. DE-AC02-06CH11357.

Supporting Information Available: HPLC and HRMS data of inhibitors and crystallographic data. This material is available free of charge via the Internet at <http://pubs.acs.org>.

References

- (1) (a) Flexner, C. HIV-protease inhibitors. *N. Engl. J. Med.* **1998**, *338*, 1281–1292. (b) Cihlar, T.; Bischofberger, N. Recent Developments

- in Antiretroviral Therapies. In *Annual Reports in Medicinal Chemistry*; Academic Press: San Diego, CA, 2000; Vol. 35, Chapter 16, pp 177–189.
- (2) Sepkowitz, K. A. AIDS, the first 20 years. *N. Engl. J. Med.* **2001**, *344*, 1764–1772.
- (3) UNAIDS/WHO Report on Annual AIDS Epidemic Update; United Nations Publications, December 2008. <http://www.unaids.org/epi/2008/>.
- (4) (a) Waters, L.; Nelson, M. Why do patients fail HIV therapy? *Int. J. Clin. Pract.* **2007**, *61*, 983–990. (b) Grabar, S.; Pradier, C.; Le Corfec, E.; Lancar, R.; Allavena, C.; Bentata, M.; Berlureau, P.; Dupont, C.; Fabbro-Peray, P.; Poizot-Martin, I.; Costagliola, D. Factors associated with clinical and virological failure in patients receiving a triple therapy including a protease inhibitor. *AIDS* **2000**, *14*, 141–149.
- (5) (a) Pillay, D.; Bhaskaran, K.; Jurriaans, S.; Prins, M.; Masquelier, B.; Dabis, F.; Gifford, R.; Nielsen, C.; Pedersen, C.; Balotta, C.; Rezza, G.; Ortiz, M.; de Mendoza, C.; Kucherer, C.; Poggensee, G.; Gill, J.; Porter, K. The impact of transmitted drug resistance on the natural history of HIV infection and response to first-line therapy. *AIDS* **2006**, *20*, 21–28. (b) Wainberg, M. A.; Friedland, G. Public health implications of antiretroviral therapy and HIV drug resistance. *JAMA, J. Am. Med. Assoc.* **1998**, *279*, 1977–1983.
- (6) Yerly, S.; Kaiser, L.; Race, E.; Bru, J. P.; Clavel, F.; Perrin, L. Transmission of antiretroviral drug resistant HIV-1 variants. *Lancet* **1999**, *354*, 729–733.
- (7) (a) Ghosh, A. K.; Kincaid, J. F.; Cho, W.; Walters, D. E.; Krishnan, K.; Hussain, K. A.; Koo, Y.; Cho, H.; Rudall, C.; Holland, L.; Buthod, J. Potent HIV protease inhibitors incorporating high-affinity P2-ligands and (R)-(hydroxyethylamino)sulfonamide isostere. *Bioorg. Med. Chem. Lett.* **1998**, *8*, 687–690. (b) Ghosh, A. K.; Shin, D.; Swanson, L.; Krishnan, K.; Cho, H.; Hussain, K. A.; Walters, D. E.; Holland, L.; Buthod, J. Structure-based design of non-peptide HIV protease inhibitors. *Farmaco* **2001**, *56*, 29–32. (c) Ghosh, A. K.; Sridhar, P. R.; Kumaragurubaran, N.; Koh, Y.; Weber, I. T.; Mitsuya, H. Bis-tetrahydrofuran: a privileged ligand for darunavir and a new generation of HIV protease inhibitors that combat drug resistance. *ChemMedChem* **2006**, *1*, 939–950.
- (8) (a) Yoshimura, K.; Kato, R.; Kavlick, M. F.; Nguyen, A.; Maroun, V.; Maeda, K.; Hussain, K. A.; Ghosh, A. K.; Gulnik, S. V.; Erickson, J. W.; Mitsuya, H. A potent human immunodeficiency virus type 1 protease inhibitor, UIC-94003 (TMC-126), and selection of a novel (A28S) mutation in the protease active site. *J. Virol.* **2002**, *76*, 1349–1358. (b) Koh, Y.; Nakata, H.; Maeda, K.; Ogata, H.; Bilcer, G.; Devasamudram, T.; Kincaid, J. F.; Boross, P.; Wang, Y. F.; Tye, Y.; Volarath, P.; Gaddis, L.; Harrison, R. W.; Weber, I. T.; Ghosh, A. K.; Mitsuya, H. Novel bis-tetrahydrofuranylurethane-containing nonpeptidic protease inhibitor (PI) UIC-94017 (TMC114) with potent activity against multi-PI-resistant human immunodeficiency virus in vitro. *Antimicrob. Agents Chemother.* **2003**, *47*, 3123–3129.
- (9) Ghosh, A. K.; Sridhar, P. R.; Leshchenko, S.; Hussain, A. K.; Li, J.; Kovalevsky, A.; Walters, D. E.; Wedekind, J. E.; Grum-Tokars, V.; Das, D.; Koh, Y.; Maeda, K.; Gatanaga, H.; Weber, I. T.; Mitsuya, H. Structure-based design of novel HIV-1 protease inhibitors to combat drug resistance. *J. Med. Chem.* **2006**, *49*, 5252–5261.
- (10) FDA approved darunavir on June 23, 2006. FDA approved new HIV treatment for patients who do not respond to existing drugs. Please see the following site: <http://www.fda.gov/bbrs/topics/NEWS/2006/NEW01395.html>.
- (11) On October 21, 2008, FDA granted traditional approval to Prezista (darunavir), coadministered with ritonavir and with other antiretroviral agents, for the treatment of HIV-1 infection in treatment-experienced adult patients. In addition to the traditional approval, a new dosing regimen for treatment-naïve patients was approved.
- (12) Ghosh, A. K.; Chapsal, B. D.; Weber, I. T.; Mitsuya, H. Design of HIV protease inhibitors targeting protein backbone: an effective strategy for combating drug resistance. *Acc. Chem. Res.* **2008**, *41*, 78–86.
- (13) Hong, L.; Zhang, X. C.; Hartsuck, J. A.; Tang, J. Crystal structure of an in vivo HIV-1 protease mutant in complex with saquinavir: insights into the mechanisms of drug resistance. *Protein Sci.* **2000**, *9*, 1898–1904.
- (14) (a) Tye, Y.; Kovalevsky, A. Y.; Boross, P.; Wang, Y. F.; Ghosh, A. K.; Tozser, J.; Harrison, R. W.; Weber, I. T. Atomic resolution crystal structures of HIV-1 protease and mutants V82A and I84V with saquinavir. *Proteins* **2007**, *67*, 232–242. (b) Kovalevsky, A. Y.; Tye, Y.; Liu, F.; Boross, P. I.; Wang, Y. F.; Leshchenko, S.; Ghosh, A. K.; Harrison, R. W.; Weber, I. T. Effectiveness of nonpeptide clinical inhibitor TMC-114 on HIV-1 protease with highly drug resistant mutations D30N, I50V, and L90M. *J. Med. Chem.* **2006**, *49*, 1379–1387.
- (15) (a) Tye, Y.; Boross, P. I.; Wang, Y. F.; Gaddis, L.; Hussain, A. K.; Leshchenko, S.; Ghosh, A. K.; Louis, J. M.; Harrison, R. W.; Weber, I. T. High resolution crystal structures of HIV-1 protease with a potent non-peptide inhibitor (UIC-94017) active against multi-drug-resistant clinical strains. *J. Mol. Biol.* **2004**, *338*, 341–352. (b) Amano, M.; Koh, Y.; Das, D.; Li, J.; Leshchenko, S.; Wang, Y. F.; Boross, P. I.; Weber, I. T.; Ghosh, A. K.; Mitsuya, H. A novel bis-tetrahydrofuranylurethane-containing nonpeptidic protease inhibitor (PI), GRL-98065, is potent against multiple-PI-resistant human immunodeficiency virus in vitro. *Antimicrob. Agents Chemother.* **2007**, *51*, 2143–2155.
- (16) (a) Ghosh, A. K.; Leshchenko, S.; Noetzel, M. Stereoselective photochemical 1,3-dioxalene addition to 5-alkoxymethyl-2(5H)-furanone: synthesis of bis-tetrahydrofuranyl ligand for HIV protease inhibitor UIC-94017 (TMC-114). *J. Org. Chem.* **2004**, *69*, 7822–7829. (b) Ghosh, A. K.; Li, J.; Ramu, S. P. A stereoselective anti-aldol route to (3R,3aS,6aR)-tetrahydro-2H-furo[2,3-b]furan-3-ol: a key ligand for a new generation of HIV protease inhibitors. *Synthesis* **2006**, 3015–3019.
- (17) (a) Ghosh, A. K.; Duong, T. T.; McKee, S. P. Di(2-pyridyl) carbonate promoted alkoxycarbonylation of amines: a convenient synthesis of functionalized carbamates. *Tetrahedron Lett.* **1991**, *32*, 4251–4254. (b) Ghosh, A. K.; Duong, T. T.; McKee, S. P.; Thompson, W. J. *N,N'*-Disuccinimidyl carbonate: a useful reagent for alkoxycarbonylation of amines. *Tetrahedron Lett.* **1992**, *33*, 2781–2784.
- (18) (a) Dondoni, A.; Perrone, D. Synthesis of 1,1-Dimethylethyl (S)-4-Formyl-2,2-dimethyl-3-oxazolidinonecarboxylate by Oxidation of the Alcohol. *Organic Syntheses*; Wiley & Sons: New York, 2004; Collect. Vol. 10, p 320. Dondoni, A.; Perrone, D. *Org. Synth.* **2000**, *77*, 64. (b) Dondoni, A.; Giovannini, P. P.; Massi, A. Assembling heterocycle-ethered C-glycosyl and α -amino acid residues via 1,3-dipolar cycloaddition reactions. *Org. Lett.* **2004**, *6*, 2929–2932.
- (19) Toth, M. V.; Marshall, G. R. A simple, continuous fluorometric assay for HIV protease. *Int. J. Pept. Protein Res.* **1990**, *36*, 544–550.
- (20) Koh, Y.; Das, D.; Leshchenko, S.; Nakata, H.; Ogata-Aoki, H.; Amano, M.; Nakayama, M.; Ghosh, A. K.; Mitsuya, H. GRL-0 2031 a novel nonpeptide protease inhibitor (PI) containing a stereochemistry defined fused cyclopentanyltetrahydrofuran (Cp-THF) potent against multi-PI-resistant HIV-1 in vitro. *Antimicrob. Agents Chemother.*, in press.
- (21) Gustchina, A.; Sansom, C.; Prevost, M.; Richelle, J.; Wodak, S.; Wlodawer, A.; Weber, I. Energy calculations and analysis of HIV-1 protease-inhibitor crystal structures. *Protein Eng.* **1994**, *7*, 309–317.
- (22) Tye, Y.; Boross, P. I.; Wang, Y. F.; Gaddis, L.; Liu, F.; Chen, X.; Tozser, J.; Harrison, R. W.; Weber, I. T. Molecular basis for substrate recognition and drug resistance from 1.1 to 1.6 Å resolution crystal structures of HIV-1 protease mutants with substrate analogs. *FEBS J.* **2005**, *272*, 5265–5277.
- (23) Panigrahi, S.; Desiraju, G. Strong and weak hydrogen bonds in the protein–ligand interface. *Proteins* **2007**, *67*, 128–141.
- (24) Steiner, T. Hydrogen bonds from water molecules to aromatic acceptors in very high-resolution protein crystal structures. *Biophys. Chem.* **2002**, *95*, 195–201.
- (25) Wang, Y. F.; Tye, Y.; Boross, P. I.; Tozser, J.; Ghosh, A. K.; Harrison, R. W.; Weber, I. T. Potent new antiviral compound shows similar inhibition and structural interactions with drug resistant mutants and wild type HIV-1 protease. *J. Med. Chem.* **2007**, *50*, 4509–4515.
- (26) Ghosh, A. K.; Gemma, S.; Baldrige, A.; Wang, Y. F.; Kovalevsky, A. Y.; Koh, Y.; Weber, I. T.; Mitsuya, H. Flexible cyclic ethers/polyethers as novel P2-ligands for HIV-1 protease inhibitors: design, synthesis, biological evaluation, and protein–ligand X-ray studies. *J. Med. Chem.* **2008**, *51*, 6021–6033.
- (27) Louis, J. M.; Clore, G. M.; Gronenborn, A. M. Autoprocessing of HIV-1 protease is tightly coupled to protein folding. *Nat. Struct. Biol.* **1999**, *6*, 868–875.
- (28) Mahalingam, B.; Louis, J. M.; Hung, J.; Harrison, R. W.; Weber, I. T. Structural implications of drug resistant mutants of HIV-1 protease: high resolution crystal structures of the mutant protease/substrate analog complexes. *Proteins* **2001**, *43*, 455–464.
- (29) Otwinowski, Z.; Minor, W. Processing of X-ray diffraction data in oscillation mode. *Methods Enzymol.* **1997**, *276*, 307–326.
- (30) Collaborative Computational Project, number 4. The CCP4 suite: programs for protein crystallography. *Acta Crystallogr.* **1994**, *D50*, 760–763.
- (31) Potterton, E.; Briggs, P.; Turkenburg, M.; Dodson, E. A graphical user interface to the CCP4 program suite. *Acta Crystallogr.* **2003**, *D59*, 1131–1137.
- (32) Sheldrick, G. M.; Schneider, T. R. SHELXL: high resolution refinement. *Methods Enzymol.* **1997**, *277*, 319–343.
- (33) Jones, T. A.; Zou, J. Y.; Cowan, S. W.; Kjeldgaard, M. Improved methods for building protein models in electron density maps and the location of errors in these models. *Acta Crystallogr.* **1991**, *A47*, 110–119.
- (34) Emsley, P.; Cowtan, K. Coot: model-building tools for molecular graphics. *Acta Crystallogr.* **2004**, *D60*, 2126–2132.
- (35) Berman, H. M.; Westbrook, J.; Feng, Z.; Gilliland, G.; Bhat, T. N.; Weissig, H.; Shindyalov, I. N.; Bourne, P. E. The Protein Data Bank. *Nucleic Acids Res.* **2000**, *28*, 235–242.

JM900303M

P-Glycoprotein Mediates Efflux Transport of Darunavir in Human Intestinal Caco-2 and ABCB1 Gene-Transfected Renal LLC-PK1 Cell Lines

Hiromi FUJIMOTO,^{a,#} Maiko HIGUCHI,^{a,#} Hiroshi WATANABE,^a Yasuhiro KOH,^b Arun K. GHOSH,^c Hiroaki MITSUYA,^b Naomi TANOUE,^a Akinobu HAMADA,^a and Hideyuki SAITO^{*,a}

^a Department of Pharmacy, Kumamoto University Hospital; ^b Department of Hematology, Kumamoto University Graduate School of Medical and Pharmaceutical Sciences, Kumamoto University; 1-1-1 Honjo, Kumamoto 860-8556, Japan;

^c Departments of Chemistry and Medicinal Chemistry, Purdue University; West Lafayette, Indiana 47907, U.S.A.

Received April 2, 2009; accepted July 4, 2009; published online July 6, 2009

Darunavir (DRV) is a nonpeptidic protease inhibitor (PI) approved for the treatment of human immunodeficiency virus (HIV) infection. DRV displays potent activity against HIV strains resistant to other available PIs. Coadministration with ritonavir (RTV) improves the oral bioavailability of DRV. Inhibition of cytochrome P450 by RTV has been proposed as a mechanism for enhanced DRV bioavailability. However, interaction of these drugs with intestinal transporters has not been elucidated. This study was performed to explore the involvement of P-glycoprotein in transcellular DRV transport in monolayers of human intestinal Caco-2 and in ABCB1 multidrug resistance 1, (MDR1) gene-transfected renal LLC-PK1 (L-MDR1) cell lines. Transepithelial transport of DRV in Caco-2 cell monolayers was 2-fold greater in the basal-to-apical direction compared to that in the opposite direction. RTV had a significant inhibitory effect on the efflux transport of DRV in Caco-2 cells. The apical-to-basal DRV transport was enhanced by P-glycoprotein inhibitors, cyclosporin A and verapamil, as well as multidrug resistance-related protein (MRP/ABCC) inhibitors, probenecid and MK571. Using the L-MDR1 cell line, basal-to-apical DRV transport was much greater than in the opposite direction. Furthermore, cyclosporin A markedly inhibited the basal-to-apical DRV transport. RTV significantly increased the apical-to-basal transport of DRV in L-MDR1 cells, but reduced transport in the opposite direction. DRV inhibited P-glycoprotein-mediated efflux of calcein-acetoxymethyl ester in L-MDR1 cells with the inhibitory potency of 121 μM . These findings suggest that DRV is a substrate of P-glycoprotein and MRP, most likely MRP2. RTV appeared to inhibit P-glycoprotein, thereby enhancing the absorptive transport of DRV.

Key words protease inhibitor; transcellular transport; P-glycoprotein; Caco-2 cell

Treatment regimens for human immunodeficiency virus (HIV) infection have been greatly improved by the development of novel classes of anti-HIV drugs, including nucleoside analogues (NRTI), non-nucleoside analogue reverse transcriptase inhibitors (NNRTI) and protease inhibitors (PI). The term highly active antiretroviral therapy (HAART) is used to describe a combination of three or more of these anti-HIV drugs.^{1,2)} During HAART, plasma HIV-1 levels rapidly decline to below the detection limit of standard clinical assays. However, reactivation of the remaining latently infected memory CD4⁺-T cells appears to be a source of continued virus reproduction.³⁾ Virologic response to HAART treatment depends on viral sensitivity to antiretroviral drugs as well as patient compliance and medication adherence.¹⁾ However, long-term HAART treatment has raised issues concerning the development of drug-resistant HIV-1 variants^{4,5)} and chronic side effects caused by the drugs.^{6,7)} With the initiation of HAART, patients generally receive a combination of two NRTIs and either NNRTI or PI. The Department of Health and Human Services recommends an initial treatment regimen with the combination of tenofovir/emtricitabine or zidovudine/lamivudine as the NRTIs and either efavirenz as an NNRTI or atazanavir with ritonavir, fosamprenavir with ritonavir (RTV), or lopinavir/RTV as the PIs.⁸⁾ However, virological failure continues to occur in a substantial proportion of HIV-infected patients who have received HAART.⁹⁾

Darunavir (DRV), formerly TMC-114, is a novel approved PI for the treatment of HIV infection.^{10,11)} It was originally designed to be active against HIV strains resistant to other

currently available PIs.¹²⁾ POWER trials have evaluated the safety and efficacy of DRV in treatment-experienced HIV patients previously given other PIs.¹³⁾ In these studies, DRV has indicated a significantly greater reduction in plasma HIV-RNA and an increase in CD4 counts compared with the active controls for patients with extensive PI resistance. Currently, there is a paucity of information on DRV resistance. Indeed, such data is mainly derived from clinical trials conducted during the registration of DRV. It is known that DRV is rapidly absorbed from the intestine after oral administration, reaching peak plasma concentrations after 2.5–4.0 h.¹⁴⁾ Absorption of DRV is followed by a fast distribution/elimination phase and a subsequent slower elimination phase with a terminal elimination half-life of 15 h in the presence of low-dose RTV as a boosting drug.^{14,15)} DRV is extensively metabolized by intestinal and hepatic cytochrome P450 (CYP) 3A4. Coadministration with small doses of RTV (100 mg) is thought to inhibit hepatic CYP3A4 activity, resulting in an increase in oral DRV bioavailability from 37 to 82%. DRV and its metabolites are mainly excreted in feces (80%), and, to a lesser extent, in urine (14%).¹⁵⁾ Most PIs are reported to suppress intestinal ABCB1/P-glycoprotein mediated drug efflux into the lumen.^{16,17)} However, there are no reports whether DRV *per se* is a transport substrate of P-glycoprotein.

The purpose of this study was to investigate the involvement of P-glycoprotein in transcellular transport of DRV across monolayers of the human intestinal epithelial Caco-2 cell line and the renal epithelial LLC-PK1 cell line stably

* To whom correspondence should be addressed. e-mail: saitohide@fc.kuh.kumamoto-u.ac.jp

These authors contributed equally to this work.

transfected with the ABCB1 gene.

MATERIALS AND METHODS

Chemicals Saquinavir (SQV) was obtained from Nippon Roche Co. (Tokyo Japan). Nelfinavir (NFV) and ritonavir (RTV) were a gift from JT Co. (Tokyo Japan) and Abbott Laboratories Co. (Illinois, U.S.A.), respectively. Darunavir (DRV) was synthesized in a convergent manner as previously described by Ghosh *et al.*¹⁰ Cyclosporin A was obtained from Novartis Pharma (Basel, Switzerland). Verapamil, probenecid, novobiocin, rifamycin SV, bromosulphophthalien, glycyllucine and glycylysarcosine were purchased from Sigma-Aldrich (St. Louis, MO, U.S.A.). MK571 was obtained from BIOMOL International, L.P. (Plymouth Meeting, PA, U.S.A.). Calcein-acetoxymethyl (AM) ester was purchased from Molecular Probe Co. (Eugene, OR, U.S.A.). All other chemicals used were of the highest purity available.

Cell Cultures Caco-2 cells at passage 18, obtained from the American Type Culture Collection (ATCC HTB37), were maintained by serial passage in plastic culture dishes as described previously.¹⁸ For the transport studies, Caco-2 cells were seeded on polycarbonate membrane filters (3- μm pores, 4.71-cm² growth area) inside Transwell cell culture chambers (Costar; Cambridge, MA, U.S.A.) at a cell density of 3×10^5 cells/well. The Transwell chambers were placed in six-well tissue culture plates with 2.6 ml of medium outside (basal chamber) and 1.5 ml of medium inside (apical chamber). The medium consisted of Dulbecco's modified Eagle's medium (Sigma-Aldrich) supplemented with 10% fetal bovine serum (BioReliance; Rockville, MD, U.S.A.) and 1% nonessential amino acids (Invitrogen; Carlsbad, CA, U.S.A.) without antibiotics. The cells were grown in an atmosphere of 5% CO₂, 95% air at 37°C, and given fresh medium every 2 or 3 d. Cells were cultured for a total of 14 d. In this study, cells between the 37th and 50th passage were used. Porcine kidney epithelial LLC-PK1 and L-MDR1 cells transfected with human ABCB1 cDNA (generous gifts from Dr. Erin G. Schuetz, St. Jude Children's Research Hospital, Memphis, TN, U.S.A.) were cultured as described previously.¹⁹ In brief, LLC-PK1 and L-MDR1 cells were maintained in complete medium consisting of Medium 199 supplemented with 10% fetal bovine serum and 1% penicillin and streptomycin, and L-MDR1 cells were maintained at 640 nM vincristine. For the transport studies, L-MDR1 and LLC-PK1 cells were seeded on polycarbonate membrane filters (3.0- μm pores, 4.71-cm² growth area) inside Transwell cell culture chambers at a cell density of 2×10^6 cells/filter. Cells in each chamber were cultured as described above for 3 d. The medium was replaced by fresh medium after 2 d, and the cells were used in the transport studies 3 d after inoculation.

Transcellular Transport and Intracellular Accumulation of DRV Transcellular transport of DRV was determined using cell monolayers grown in Transwell chambers. Culture medium on either the basal or apical side of the monolayers was replaced with 2 ml of incubation medium [145 mM NaCl, 3 mM KCl, 1 mM CaCl₂, 0.5 mM MgCl₂, 5 mM D-glucose, 8 mM Na₂HPO₄, 1.5 K₂HPO₄ and 5 mM N-(2-hydroxyethyl)piperazine-*N'*-2-ethanesulfonic acid (HEPES) (pH 7.4) or MES (pH 6.0)] containing DRV (10 μM) with or without PI, and medium on the opposite side was replaced

with 2 ml of fresh incubation medium. In inhibition study, an inhibitor was added to the incubation medium on both sides of the monolayer. The monolayers were incubated in 5% CO₂-95% air at 37°C for up to 6 h, and 130 μl aliquots of medium from the relevant side were taken at the indicated time points. For accumulation studies, the medium was aspirated off at the end of the incubation period, and the monolayers were washed twice with 2 ml of ice-cold incubation medium. The filters with cell monolayers were immersed in 1 ml of extraction solution composed of the mobile phase of HPLC assay/methanol (1:1) for 1 h. Supernatants obtained after centrifugation at 200 g for 15 min were used for the HPLC assay. The remaining cells were lysed with 1 ml of 1 N NaOH, and used for the protein assay using a Bio-Rad protein assay kit (Bio-Rad Laboratories; Richmond, CA, U.S.A.) with bovine γ -globulin as a standard.

Calcein-AM Efflux Assay Efflux assays were performed as described previously.¹⁹ A kinetic fluorometric assay was used to study the interaction of DRV with P-glycoprotein. For the calcein-AM efflux assay, L-MDR1 and LLC-PK1 cells were seeded in 96-well tissue culture plates at a cell density of 1×10^5 cells/well. Cells were cultured in 200 μl of Medium 199 supplemented with 10% fetal bovine serum in each well in an atmosphere of 5% CO₂-95% air at 37°C for 1 d. Cells were plated in 96-well tissue culture plates in Medium 199 containing PI. After a 30-min incubation period, calcein-AM was added to a final concentration of 2 μM , and the plates were placed into a Fluoroscan Ascent Thermo Labsystems, Franklin, MA, U.S.A.). Fluorescence was measured from 0 to 30 min using an excitation of 485 nm and an emission of 530 nm. The rate of calcein accumulation in the presence and absence of DRV was calculated by linear regression analysis using the Ascent software (Thermo Labsystems). Inhibitory potency of DRV for P-glycoprotein was evaluated by fluorescence at 30 min as a percentage of LLCmax, $((\text{L-MDR1}[\text{I}]) - (\text{L-MDR1}[\text{0}])) \times 100 / ((\text{LLC-PK1}[\text{0}]) - (\text{L-MDR1}[\text{0}]))$, where [I] represents a concentration of DRV, and [0] means absence of DRV.²⁰

HPLC Determination of DRV The concentration of DRV was determined using HPLC (model LC-6A; Shimadzu, Kyoto, Japan). One hundred ml of sample were injected into the HPLC column. Separation was performed on a reversed-phase column (Zorbax SB-C18, 5- μm particle size, 150 mm \times 4 mm i.d.) at 40°C. The mobile phase was a mixture of solution containing 25 mM sodium acetate and 25 mM hexane-1-sulfuric acid (pH 6.0) and acetonitrile (57:43). The flow rate was 1.0 ml/min and DRV was detected by UV absorption at 268 nm. The recovery of known small amount of DRV applied on cell monolayers for 60 min in the extraction method was >93%.

Statistical Analysis Data were analyzed statistically by analysis of variance (ANOVA) followed by Scheffe's multiple comparison test. A *p*-value of less than 0.05 was considered statistically significant.

RESULTS

Effect of RTV on the Transepithelial Transport of DRV in Caco-2 Cell Monolayers Transepithelial transport of DRV (10 μM) in the apical-to-basal direction was time-dependent. Approximately 20% of the applied DRV in the api-

cal chamber permeated into the basal compartment after 6 h (Fig. 1). The basal-to-apical transport of DRV was also time-dependent, with 43% of the applied DRV dose found in the opposite compartment after 6 h. These findings suggest that transepithelial transport of DRV is two-fold greater in the basal-to-apical direction compared to the opposite direction, corresponding to intestinal secretory transport. The apical-to-basal transport of DRV in the presence of RTV (20 μ M) was significantly elevated compared to that in the absence of RTV. In contrast, the basal-to-apical transport of DRV was unaffected by the presence of RTV. The results indicate that

the presence of RTV in the apical compartment had an inhibitory effect on efflux transport of DRV in the apical membranes of Caco-2 cells. The apical-to-basal transport of DRV in the presence of either cyclosporin A or verapamil, representative inhibitors of P-glycoprotein, was significantly increased compared to that in the absence of inhibitors (data not shown).

Effects of Various Inhibitors on Transcellular Transport of DRV in Caco-2 Cell Monolayers The apical-to-basal transport of DRV was significantly increased in the presence of cyclosporin A, verapamil, probenecid, MK571, rifamycin SV and bromosulfophthalein (BSP) (Fig. 2). Probenecid and MK571 have been reported to inhibit multidrug resistant-associated protein (MRP/ABCC) 2.²² Rifamycin SV and BSP are known to inhibit organic anion transporting protein (OATP/SLCO) family members OATP1B1 and OATP1B3, respectively.²³ In contrast, novobiocin, an inhibitor for breast cancer resistance protein (BCRP/ABCG2),²⁴ significantly enhances the basal-to-apical transport of DRV. Glycyllucine and glycyllsarcosine, a substrate and inhibitor of H⁺/oligopeptide cotransporter PEPT1 (SLC15A1), respectively,¹⁸ had no effect on the DRV transport. The ratio of basal-to-apical transport to apical-to-basal transport indicates that cyclosporin A, verapamil and RTV strongly suppressed the net secretory transepithelial transport of DRV. Probenecid, MK571 rifamycin SV and BSP had weak but significant inhibitory effects on the secretory transport of DRV. However, novobiocin markedly stimulated the secretory transport of DRV.

Effect of Cyclosporin A and Verapamil on Transepithe-

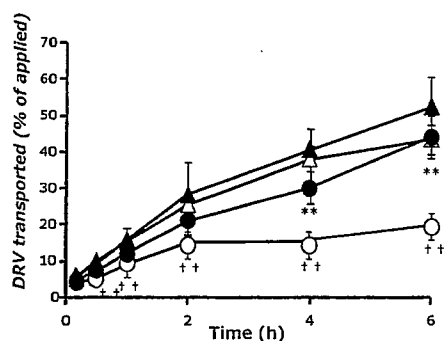


Fig. 1. Effect of RTV on the Transepithelial Transport of DRV in Monolayers of Caco-2 Cells

Transport of DRV (10 μ M) in the apical-to-basal direction (O, ●) and in the basal-to-apical direction (Δ , \blacktriangle) in the absence (control, open symbol) or presence (closed symbol) of RTV (20 μ M). Each point represents the mean \pm S.D. of three independent measurements. ** p < 0.01, significantly different from apical-to-basal transport without RTV. † p < 0.01, significantly different from basal-to-apical transport without RTV.

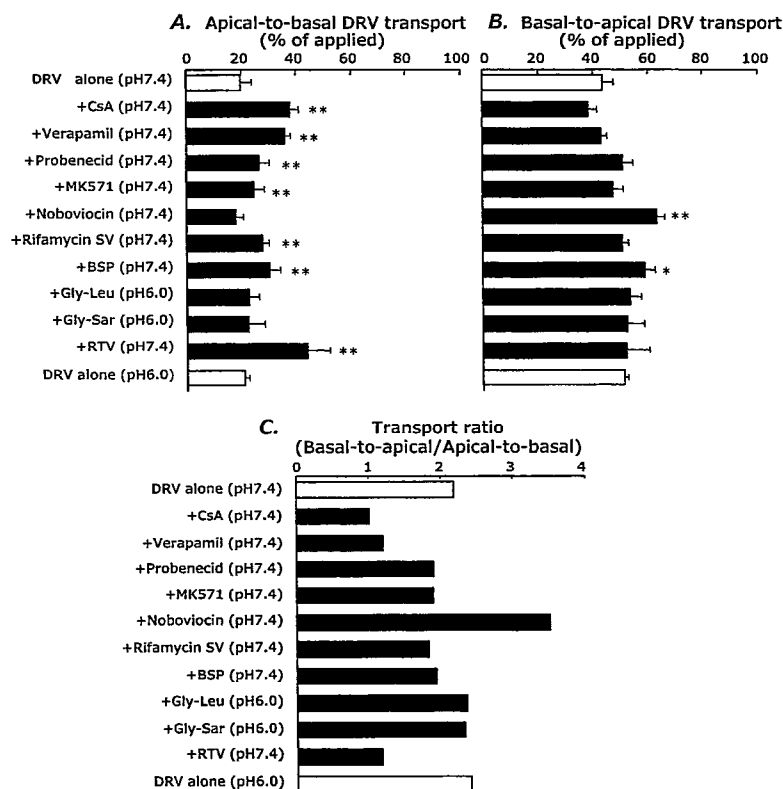


Fig. 2. Effect of Various Inhibitors on Transepithelial Transport of DRV in Monolayers of Caco-2 Cells 6 h after Incubation with DRV

Apical-to-basal transport (A), basal-to-apical transport (B) and the transport ratio of basal-to-apical transport divided by apical-to-basal transport (C). Each bar represents the mean \pm S.D. of three independent measurements. * p < 0.05, ** p < 0.01; significantly different from control (DRV alone).

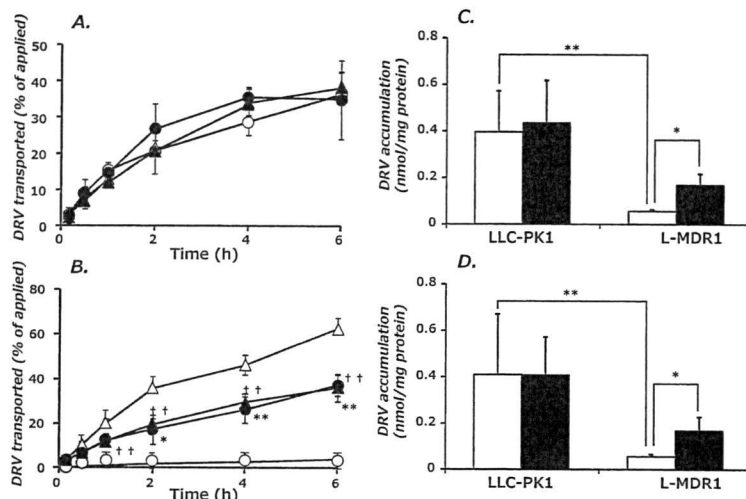


Fig. 3. Transepithelial Transport and Intracellular Accumulation of DRV in LLC-PK1 Cells and L-MDR1 Cells

Transport of DRV (10 μM) in the apical-to-basal direction (O, ●) and in the basal-to-apical direction (Δ , \blacktriangle) in the absence (control, open symbol) or presence (closed symbol) of cyclosporin A (10 μM) in LLC-PK1 (A) or L-MDR1 (B) cells. Each point represents the mean \pm S.D. of three independent measurements. ** $p < 0.01$, * $p < 0.05$, significantly different from apical-to-basal transport without cyclosporin A. † $p < 0.01$, significantly different from basal-to-apical transport without cyclosporin A. Intracellular accumulation of DRV in the absence (control, open column) and presence of cyclosporin A (closed column) 6 h after addition of DRV (10 μM) to the apical side (C) and basal side (D) of the monolayer. Each point represents the mean \pm S.D. of three independent measurements. ** $p < 0.01$, significantly different from DRV accumulation in LLC-PK1 cells without cyclosporin A. * $p < 0.05$, significantly different from DRV accumulation in L-MDR1 cells without cyclosporin A.

lial Transport of DRV in LLC-PK1 and L-MDR1 Cells

P-glycoprotein is an efflux pump responsible for limiting the oral bioavailability and tissue penetration of saquinavir.²⁵⁾ In order to confirm the involvement of P-glycoprotein in DRV transport, we compared transepithelial transport of DRV in untransfected renal LLC-PK1 cells and ABCB1/MDR1 gene-transfected LLC-PK1 (L-MDR1) cells overexpressing P-glycoprotein in the apical membrane domain. As shown in Fig. 3A, there was no difference in the transport of DRV between the apical-to-basal and basal-to-apical directions in the LLC-PK1 cell monolayers. However, the basal-to-apical transport of DRV was much greater than the apical-to-basal transport in L-MDR1 cell monolayers. Furthermore, cyclosporin A markedly decreased the basal-to-apical transport and increased apical-to-basal transport of DRV in L-MDR1 cells (Fig. 3B). Figures 3C and D show the intracellular accumulation of DRV after incubation with the drug on either the apical or basal side of the monolayer in the presence and absence of cyclosporin A. In all cases, the accumulation of DRV was much lower in L-MDR1 cells in comparison to LLC-PK1 cells. Cyclosporin A significantly increased the accumulation of DRV from both sides of the monolayer. These findings suggest that transepithelial transport of DRV is stimulated *via* P-glycoprotein in L-MDR1 cells.

Inhibitory Effects of PIs on Transepithelial Transport of DRV in L-MDR1 Cells

NFV markedly enhanced the apical-to-basal transport of DRV, but suppressed the basal-to-apical transport (Figs. 4A, 4B). RTV or SQV at a concentration of 50 μM significantly increased apical-to-basal DRV transport and decreased DRV transport in the opposite direction. Net secretory transport, evaluated as the ratio of basal-to-apical to apical-to-basal transport, showed NFV to have a potent inhibitory effect on P-glycoprotein-mediated transport of DRV when compared to RTV and SQV (Fig. 4C). RTV and SQV showed inhibitory effects on the net secretory transport of DRV at a concentration of 50 μM .

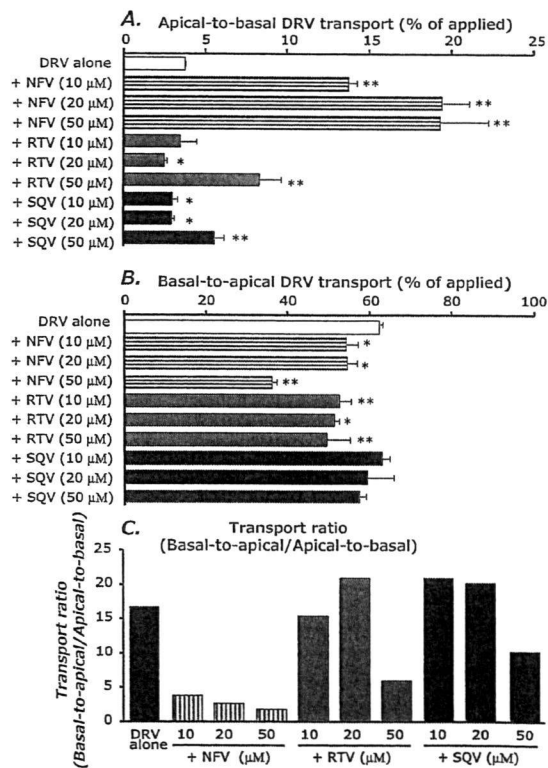


Fig. 4. Effect of PIs on the Transepithelial Transport of DRV in L-MDR1 Cells 6 h after Incubation with DRV

Transport of DRV (10 μM) in the apical-to-basal direction (A) or basal-to-apical direction (B). The transport ratio (basal-to-apical/apical-to-basal) is given in (C). Each point represents the mean \pm S.D. of three independent measurements. ** $p < 0.01$, * $p < 0.05$, significantly different from control (DRV alone).

Inhibitory Effect of DRV on P-Glycoprotein-Mediated

Calcein-AM Efflux In order to evaluate inhibitory effects of DRV on P-glycoprotein transport activity, calcein-AM ex-

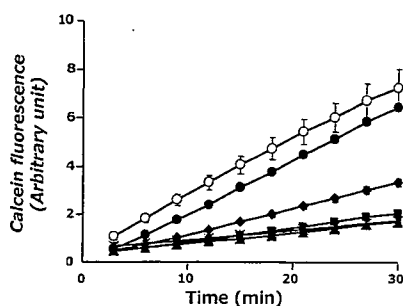


Fig. 5. The Effect of DRV on Intracellular Uptake of Calcein-AM in LLC-PK1 and L-MDR1 Cells Monolayers

LLC-PK1 cells without DRV (O), L-MDR1 cells without DRV (X), L-MDR1 cells with DRV at concentrations of 10 μM (\blacktriangle), 25 μM (\blacksquare), 50 μM (\blacklozenge) and 100 μM (\bullet). Each point represents the mean \pm S.D. of five independent measurements.

trusion test was performed using LLC-PK1 and L-MDR1 cells. As shown in Fig. 5, cellular accumulation of calcein was time dependent. Calcein accumulated much faster in LLC-PK1 cells than in L-MDR1 cells, confirming that calcein-AM was actively excluded in L-MDR1 cells by P-glycoprotein. RTV increased calcein accumulation in a dose-dependent manner in L-MDR1 cells, suggesting inhibition of P-glycoprotein activity. LLCmax of DRV was 121 μM and this potent inhibitory effect was comparable to that of RTV (LLCmax = 111 μM).²⁰

DISCUSSION

It has been reported that most of the currently available PIs are transport substrates of P-glycoprotein.^{25,26} P-glycoprotein expressed in intestinal epithelial cells is thought to decrease absorption of orally administered PIs. Low levels of intestinal absorption together with CYP P450 activity are major factors in the first-pass effect of these drugs.^{16,26} For example, it was reported that the area under the time-plasma concentration curves (AUC) after oral administration of SQV in *mdr1*-knockout mice was elevated five-fold compared to that of wild-type mice.²⁷ Moreover, Meaden *et al.* reported that P-glycoprotein expression levels in lymphocytes of patients coadministered with RTV and SQV were negatively correlated with the cellular accumulation of these PIs.²¹ It was also suggested that P-glycoprotein expressed in the blood-brain barrier and blood-placenta barrier participate in the restricted distribution of indinavir, SQV, NFV or amprenavir into the brain and placenta, respectively.^{28,29} Therefore, P-glycoprotein is thought to play a key role in the pharmacokinetics and therapeutic efficacy of most PIs. It was reported that DRV had a weak inhibitory effect ($\text{IC}_{50} > 100 \mu\text{M}$) on P-glycoprotein expressed in *MDR1*-gene transfected Madin-Darby canine kidney (MDCK) cells.³⁰ However, it was not known whether DRV is recognized by P-glycoprotein as a transport substrate.

We explored transcellular transport of DRV using Caco-2 cells, which have been demonstrated to express ATP-binding cassette (ABC) transporter family members including ABCB1/P-glycoprotein, MRPs (ABCC2-6) and BCRP, OATP (SLCO) family members OATP-A and OATP-B, organic cation transporter OCT1 (SLC22A1), and organic anion transporter OAT2 (SLC22A7).^{22,31-33} In the present

study, typical P-glycoprotein inhibitors, cyclosporin A and verapamil, enhanced the apical-to-basal transport of DRV in Caco-2 cells, suggesting that P-glycoprotein mediates efflux transport of DRV in the apical membranes of Caco-2 cells. The ratio of basal-to-apical to apical-to-basal transport was approximately 2.2, indicating that net secretory transport of DRV is preferred in Caco-2 epithelial cells. Probenecid and MK571, nonspecific MRP inhibitors, also had significant but much weaker effects on the apical-to-basal transport of DRV in Caco-2 cells. Huisman *et al.* reported that indinavir, SQV and RTV were transported by MRP2, but not by MRP1 and MRP3.³⁴ Moreover, Williams *et al.* reported that SQV could be a substrate for P-glycoprotein, MRP1 and MRP2 with the transportability of P-glycoprotein > MRP2 > MRP1.³⁵ Therefore, our results suggest that MRP2 could mediate, at least in part, the apical efflux of DRV in Caco-2 cells. Novobiocin, a typical BCRP inhibitor,²⁴ stimulated the basal-to-apical transport of DRV in Caco-2 cells. This finding suggests that BCRP is not involved in the transcellular transport of DRV, because BCRP is localized in the apical membranes of Caco-2 cells where it mediates efflux of substrates. However, we cannot exclude the possibility that unidentified novobiocin-sensitive transporter(s) expressed in the basolateral membranes of Caco-2 cells may also mediate the efflux transport of DRV. The OATP non-specific inhibitors, rifamycin SV and BSP,^{32,33} showed weak but significant stimulatory effects on the apical-to-basal transport. Interestingly, this represents the opposite net direction of transport for DRV, suggesting a partial involvement of OATP-A and/or OATP-B in transcellular transport of this drug in Caco-2 cells. In the inhibition studies with glycyllucine and glycy sarcosine, we found no contribution of PEPT1 to apical DRV transport in Caco-2 cells. These findings suggest that P-glycoprotein mediates predominantly efflux transport of DRV in the apical membranes of Caco-2 cells, but other apical membrane-localized efflux transporters MRP2 and/or BCRP, and also OATP might be involved, at least in part, in transcellular transport of DRV.

The present work using L-MDR1 cells provides the first direct evidence that DRV is a transport substrate of P-glycoprotein. The inhibitory potency of DRV was comparable to that of RTV. In HIV therapy, the bioavailability of DRV (100 mg two times a day) is improved by oral coadministration with RTV (600 mg) *i.e.*, from 37% for DRV alone to 82% in combination with RTV.¹⁵ It is generally thought that the boosting effect of RTV is due to the inhibition of oxidative metabolism in the intestine and liver by specifically targeting CYP3A4 activity.¹⁵ Indeed, the apparent inhibition constant (K_i) of RTV for CYP3A4 and human hepatic microsomes were reported to be 0.10 μM and 0.17 μM , respectively, suggesting RTV is a potent inhibitor of CYP3A4.³⁶ However, our results demonstrate that the mechanisms of action of RTV in terms of improving the bioavailability of DRV involve inhibition of the efflux transport systems of the intestinal lumen in addition to the intestinal/hepatic metabolism. Further investigation is required in order to explore the relative contribution of these two mechanisms towards the improvement of oral bioavailability of DRV in clinical treatment.

In conclusion, the present study has revealed that DRV is a transport substrate of P-glycoprotein in Caco-2 cells and in *MDR1* gene-transfected renal LLC-PK1 cells. MRP, most

likely MRP2, was found to be partially involved in the apical efflux transport of DRV in Caco-2 cells. Furthermore, our results suggest RTV inhibits P-glycoprotein, thereby enhancing the apical-to-basal transport (*i.e.*, absorptive pathway) of DRV.

Acknowledgements This work was supported in part by a Grant-in-Aid for Scientific Research from the Japan Society for the Promotion of Science (JSPS) for Hideyuki Saito (KAKENHI 17390158) and Akinobu Hamada (KAKENHI 19590149).

REFERENCES

- Bartlett J. A., Fath M. J., Demasi R., Hermes A., Quinn J., Mondou E., Rousseau F., *AIDS*, **20**, 2051—2064, (2006).
- Piacenti F. J., *Pharmacotherapy*, **26**, 1111—1133 (2006).
- Belmonte L., Baré P., de Bracco M. M., Ruibal-Ares B. H., *Curr. Med. Chem.*, **10**, 303—312 (2003).
- Kozal M. J., Hullsiek K. H., Macarthur R. D., Berg-Wolf M., Peng G., Xiang Y., Baxter J. D., Uy J., Telzak E. E., Novak R. M., *HIV Clin. Trials*, **8**, 357—370 (2007).
- Siliciano J. D., Siliciano R. F., *J. Antimicrob. Chemother.*, **54**, 6—9 (2004).
- Barbaro G., *Am. J. Ther.*, **13**, 248—260 (2006).
- Haugaard S. B., *Expert Opin. Drug Metab. Toxicol.*, **2**, 429—445 (2006).
- Boyle B. A., *AIDS Read.*, **14**, 71—74 (2004).
- Røge B. T., Barfod T. S., Kirk O., Katzenstein T. L., Obel N., Nielsen H., Pedersen C., Mathiesen L. R., Lundgren J. D., Gerstoft J., *HIV Med.*, **5**, 344—351 (2004).
- Ghosh A. K., Sridhar P. R., Leshchenko S., Hussain A. K., Li J., Kovalevsky A. Y., Walters D. E., Wedekind J. E., Grum-Tokars V., Das D., Koh Y., Maeda K., Gatanaga H., Weber I. T., Mitsuya H., *J. Med. Chem.*, **49**, 5252—5261 (2006).
- Koh Y., Matsumi S., Das D., Amano M., Davis D. A., Li J., Leschenko S., Baldridge A., Shioda T., Yarchoan R., Ghosh A. K., Mitsuya H., *J. Biol. Chem.*, **282**, 28709—28720 (2007).
- Mitsuya H., Maeda K., Das D., Ghosh A. K., *Adv. Pharmacol.*, **56**, 169—197 (2008).
- Clotet B., Bellos N., Molina J. M., Cooper D., Goffard I. C., Lazzarin A., Wöhrmann A., Katlama C., Wilkin T., Haubrich R., Cohen C., Farthing C., Jayaweera D., Markowitz M., Ruane P., Spinoso-Guzman S., Lefebvre E., *Lancet*, **369**, 1169—1178 (2007).
- Boffito M., Winston A., Jackson A., Fletcher C., Pozniak A., Nelson M., Moyle G., Tolowinska I., Hoetelmans R., Miralles D., Gazzard B., *AIDS*, **21**, 1449—1455 (2007).
- Rittweger M., Arastéh K., *Clin. Pharmacokinet.*, **46**, 739—756 (2007).
- Benet L. Z., Izumi T., Zhang Y., Silverman J. A., Wacher V. J., *J. Controlled Release*, **62**, 25—31 (1999).
- Lee C. G., Gottesman M. M., Cardarelli C. O., Ramachandra M., Jeang K. T., Ambudkar S. V., Pastan I., Dey S., *Biochemistry*, **37**, 3594—3601 (1998).
- Saito H., Inui K., *Am. J. Physiol.*, **265**, G289—G294 (1993).
- Hamada A., Miyano H., Watanabe H., Saito H., *J. Pharmacol. Exp. Ther.*, **307**, 824—828 (2003).
- Shiraki N., Hamada A., Yasuda K., Fujii J., Arimori K., Nakano M., *Biol. Pharm. Bull.*, **23**, 1528—1531 (2000).
- Meaden E. R., Hoggard P. G., Newton P., Tjia J. F., Aldam D., Cornforth D., Lloyd J., Williams I., Back D. J., Khoo S. H., *J. Antimicrob. Chemother.*, **50**, 583—588 (2002).
- Hirohashi T., Suzuki H., Chu X. Y., Tamai I., Tsuji A., Sugiyama Y., *J. Pharmacol. Exp. Ther.*, **292**, 265—270 (2000).
- Vavricka S. R., Van Montfort J., Ha H. R., Meier P. J., Fattinger K., *Hepatology*, **36**, 164—172 (2002).
- Shiozawa K., Oka M., Soda H., Yoshikawa M., Ikegami Y., Tsurutani J., Nakatomi K., Nakamura Y., Doi S., Kitazaki T., Mizuta Y., Murase K., Yoshida H., Ross D. D., Kohno S., *Int. J. Cancer*, **108**, 146—151 (2004).
- Jain R., Agarwal S., Majumdar S., Zhu X., Pal D., Mitra A. K., *Int. J. Pharm.*, **303**, 8—19 (2005).
- Kim R. B., Fromm M. F., Wandel C., Leake B., Wood A. J., Roden D. M., Wilkinson G. R., *J. Clin. Invest.*, **101**, 289—294 (1998).
- Park S., Sinko P. J., *J. Pharmacol. Exp. Ther.*, **312**, 1249—1256 (2005).
- Anderson B. D., May M. J., Jordan S., Song L., Roberts M. J., Leggs M., *Drug Metab. Dispos.*, **34**, 653—659 (2006).
- Salama N. N., Kelly E. J., Bui T., Ho R. J., *J. Pharm. Sci.*, **94**, 1216—1225 (2005).
- Tong L., Phan T. K., Robinson K. L., Babusis D., Strab R., Bhoopathy S., Hidalgo I. J., Rhodes G. R., Ray A. S., *Antimicrob. Agents Chemother.*, **51**, 3498—3504 (2007).
- Englund G., Rorsman F., Rönnblom A., Karibom U., Lazorova L., Gråsjö J., Kindmark A., Artursson P., *Eur. J. Pharm. Sci.*, **29**, 269—277 (2006).
- Sai Y., Kaneko Y., Ito S., Mitsuoka K., Kato Y., Tamai I., Artursson P., Tsuji A., *Drug Metab. Dispos.*, **34**, 1423—1431 (2006).
- Seithel A., Karlsson J., Hilgendorf C., Björquist A., Ungell A. L., *Eur. J. Pharm. Sci.*, **28**, 291—299 (2006).
- Huisman M. T., Smit J. W., Crommentuyn K. M., Zelcer N., Wiltshire H. R., Beijnen J. H., Schinkel A. H., *AIDS*, **16**, 2295—2301 (2002).
- Williams G. C., Liu A., Knipp G., Sinko P. J., *Antimicrob. Agents Chemother.*, **46**, 3456—3462 (2002).
- Ernest C. S., Hall S. D., Jones D. R., *J. Pharmacol. Exp. Ther.*, **312**, 583—591 (2005).

Design, Synthesis, Protein–Ligand X-ray Structure, and Biological Evaluation of a Series of Novel Macrocyclic Human Immunodeficiency Virus-1 Protease Inhibitors to Combat Drug Resistance[†]

Arun K. Ghosh,^{*,‡} Sarang Kulkarni,[‡] David D. Anderson,[‡] Lin Hong,[§] Abigail Baldrige,[‡] Yuan-Fang Wang,[‡] Alexander A. Chumanevich,[‡] Andrey Y. Kovalevsky,[‡] Yasushi Tojo,[#] Masayuki Amano,[#] Yasuhiro Koh,[#] Jordan Tang,^{§,||} Irene T. Weber,[‡] and Hiroaki Mitsuya^{#,∇}

[‡]Departments of Chemistry and Medicinal Chemistry, Purdue University, West Lafayette, Indiana 47907, [§]Protein Studies Program, Oklahoma Medical Research Foundation, Oklahoma City, Oklahoma 73104, ^{||}Department of Biochemistry and Molecular Biology, University of Oklahoma Health Science Center, Oklahoma City, Oklahoma 73104, [∇]Department of Biology, Molecular Basis of Disease, Georgia State University, Atlanta, Georgia 30303, [#]Departments of Hematology and Infectious Diseases, Kumamoto University School of Medicine, Kumamoto 860-8556, Japan, and [†]Experimental Retrovirology Section, HIV and AIDS Malignancy Branch, National Cancer Institute, Bethesda, Maryland 20892

Received May 22, 2009

The structure-based design, synthesis, and biological evaluation of a series of nonpeptidic macrocyclic HIV protease inhibitors are described. The inhibitors are designed to effectively fill in the hydrophobic pocket in the S1'–S2' subsites and retain all major hydrogen bonding interactions with the protein backbone similar to darunavir (**1**) or inhibitor **2**. The ring size, the effect of methyl substitution, and unsaturation within the macrocyclic ring structure were assessed. In general, cyclic inhibitors were significantly more potent than their acyclic homologues, saturated rings were less active than their unsaturated analogues and a preference for 10- and 13-membered macrocyclic rings was revealed. The addition of methyl substituents resulted in a reduction of potency. Both inhibitors **14b** and **14c** exhibited marked enzyme inhibitory and antiviral activity, and they exerted potent activity against multidrug-resistant HIV-1 variants. Protein–ligand X-ray structures of inhibitors **2** and **14c** provided critical molecular insights into the ligand-binding site interactions.

Introduction

HIV/AIDS has become one of the major medical and humanitarian challenges in the 21st century.¹ Highly active antiretroviral therapy (HAART[®]), which combines protease inhibitors along with reverse-transcriptase inhibitors, is currently used to combat this pandemic. HAART therapy has resulted in a significant decline in the number of deaths due to HIV infection in the developed countries.² One of the major challenges still faced is the emergence of drug-resistant viral strains rendering the present drug regimens ineffective.³ There is an urgent need for development of antiretroviral agents with minimal side effects and broad-spectrum activity for current and future management of HIV/AIDS.

Recently, our structure-based design of inhibitors maximizing interactions within the active site protease backbone led to the development of nonpeptide inhibitors (**1**–**2**) that have shown picomolar enzyme affinity and exceptional antiviral activity against both wild-type and drug-resistant HIV-1 strains.^{4–6} The X-ray crystallographic studies revealed that the backbone conformation of mutant protease is minimally distorted compared to wild-type HIV-1 proteases. We, therefore,

speculated that maximizing “backbone binding” may be an important design strategy to combat drug resistance.⁷ Inhibitor **1** (darunavir, TMC-114) was recently approved by the FDA for the treatment of drug-resistant HIV strains.⁸ More recently, it has been approved for all HIV/AIDS patients including pediatric AIDS patients.⁹ The protein–ligand X-ray structure of darunavir and its analogue **2** (TMC-126) exhibited extensive hydrogen bonding interactions with the backbone atoms throughout the active site of the HIV-1 protease.^{10,11}

In our continuing efforts toward the conceptual design of novel PIs, we now plan to design PIs with functionalities that interact with the protein backbone as well as introduce flexible macrocycles involving P1'–P2' ligands for effective repacking due to side chain mutations. The notion of such macrocyclic design evolved from the observation that certain mutations lead to decreased van der Waals interactions and increased the size of the S1 hydrophobic pocket. The X-ray structure and modeling studies of PI (2*S*,2'*S*)-*N,N'*-((2*S*,3*R*,4*R*,5*S*)-3-hydroxy-4-methyl-1,6-diphenylhexane-2,5-diyl)bis(3-methyl-2-(3-methyl-3-(pyridin-2-ylmethyl)ureido)butanamide) (A-77003)¹² indicated that the V82A mutant results in decreased van der Waals interactions with the phenyl rings in both the S1 and S1'-subsites.¹³ There was also evidence of repacking of inhibitor side chains and enzyme atoms in the S1-subsite. On the basis of this insight of enzyme flexibility in accommodating alternate packing, we planned to design flexible macrocycles between the P1' side chain and the P2' sulfonamide ring to fill in the S1' and S2'-subsites.¹³ In particular, we envisioned

[†]The PDB accession code for 2-bound HIV-1 protease X-ray structure is 3I7E and 14c-bound HIV-1 protease X-ray structure is 3I6O.

*To whom correspondence should be addressed. Phone: (765)-494-5323. Fax: (765)-496-1612. E-mail: akghosh@purdue.edu.

[®]Abbreviations: HIV, human immunodeficiency virus; bis-THF, bis-tetrahydrofuran; PI, protease inhibitor; HAART, highly active antiretroviral therapy; APV, amprenavir; DRV, darunavir; SQV, saquinavir; IDV, indinavir; LPV, lopinavir; DIAD, diisopropyl azodicarboxylate.

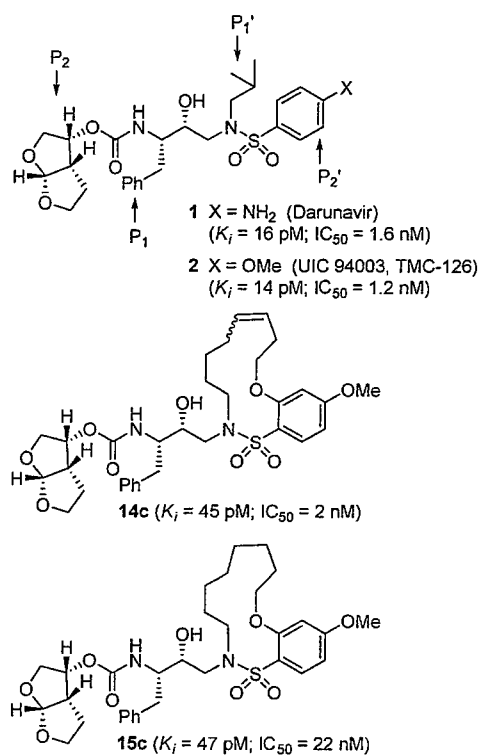
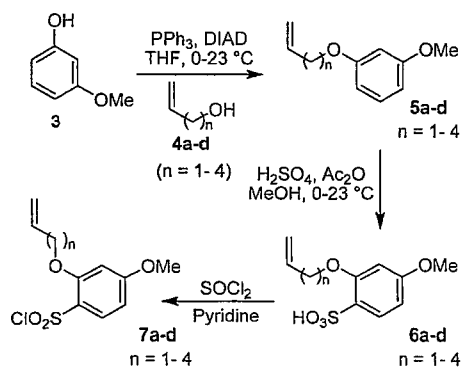


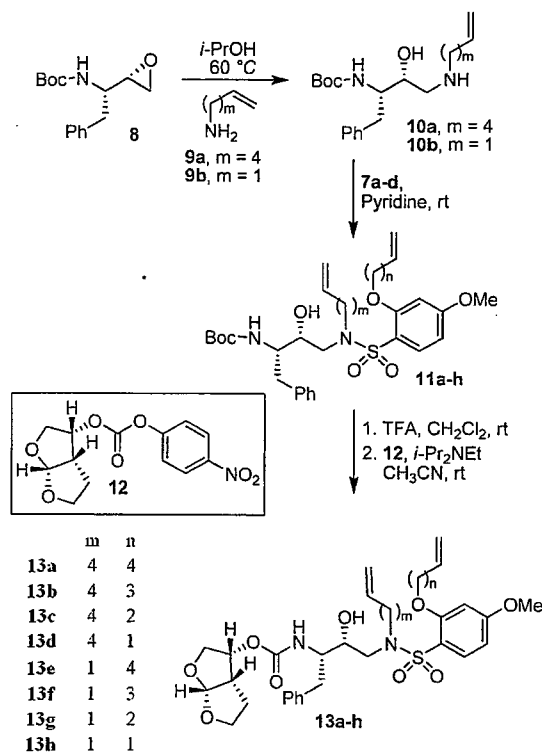
Figure 1. Structure of inhibitors 1, 2, 14c, and 15c.

Scheme 1. Synthesis of Sulfonyl Chlorides 7a–d



that 11–15-membered saturated and unsaturated macrocycles would effectively fill in the S1'–S2' hydrophobic pocket of the enzyme active site while retaining all major interactions of PIs 1 and 2 with the protein backbone. Conceivably, such inhibitors will maintain potency against both wild-type and mutant strains. On the basis of this presumption, we designed a series of PIs that incorporated various macrocycles that could effectively fill in the enzyme active site. Herein we report the structure-based design, synthesis, and preliminary biological results of these macrocyclic inhibitors. Among these compounds, 14b and 14c were the most potent, with both excellent enzyme inhibitory and antiviral activity. Both inhibitors exerted potent activity against multidrug-resistant HIV-1 variants. Furthermore, protein–ligand X-ray structures of inhibitors 2- and 14c-bound HIV-1 protease have revealed important insights regarding ligand-binding interactions (Figure 1).

Scheme 2. Synthesis of Compounds 13a–h



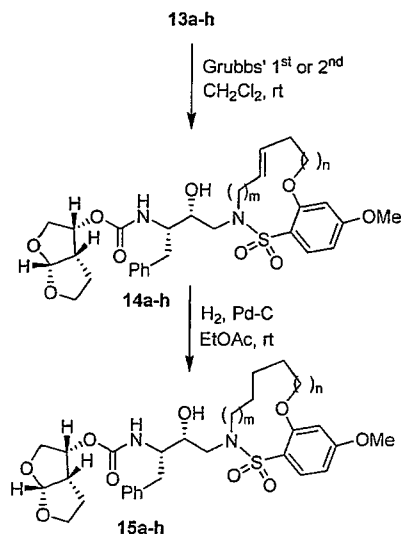
Chemistry

The synthesis of sulfonyl chlorides 7a–d is shown in Scheme 1. A Mitsunobu-type reaction between 3-methoxyphenol and alcohols 4a–d in the presence of triphenylphosphine and diisopropyl azodicarboxylate (DIAD) afforded the ethers 5a–d.¹⁴ Electrophilic aromatic substitution of ethers 5a–d with acetic anhydride and concentrated sulfuric acid in methanol furnished a mixture of sulfonic acid regioisomers in a 1:1 ratio that were separated by flash chromatography to give 6a–d. Structural confirmation of the isomers was determined by extensive 2D NMR experiments (NOESY and HMBC). Conversion to the sulfonyl chlorides 7a–d was achieved by reaction of the sulfonic acids 6a–d with thionyl chloride in the presence of pyridine.

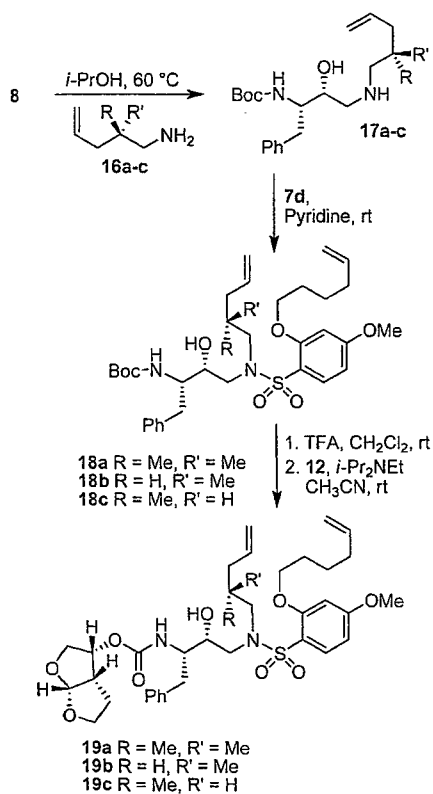
The synthesis of compounds 13a–h is outlined in Scheme 2. Nucleophilic attack of amines 9a and 9b on commercially available epoxide 8 in the presence of isopropyl alcohol gave hydroxy amines 10a and 10b. The conversion of amines 10a and 10b to the sulfonamides 11a–h was realized by coupling with sulfonyl chlorides 7a–d in the presence of pyridine. Removal of the Boc protecting group from sulfonamides 11a–h using 30% trifluoroacetic acid in CH₂Cl₂ furnished the corresponding amines, which were then coupled with activated bis-THF¹⁵ (12) to give acyclic inhibitors 13a–h.

The acyclic compounds 13a–h thus obtained were exposed to ring closing metathesis using Grubbs' first- or second-generation catalyst¹⁶ (Scheme 3) to give the unsaturated macrocyclic inhibitors 14a–h. Interestingly, larger ring sizes (15–13) gave a mixture of *E/Z* isomers, while in the case of smaller rings (12–9), the *Z* isomer was obtained exclusively. The *E* and *Z* isomers were isolated using reversed-phase HPLC and the stereochemistry established by 2D NMR

Scheme 3. Synthesis of Macrocyclic Inhibitors 14a–h and 15a–h



Scheme 4. Synthesis of Compounds 19a–c



(COSY and NOESY) experiments, allowing their individual biological evaluation. The unsaturated compounds were subsequently reduced using hydrogen and 10% Pd-C as the catalyst to yield inhibitors 15a–h.

A series of selectively methylated inhibitors were prepared in a similar fashion. Nucleophilic attack of amines 16a–c on commercially available epoxide 8 gave hydroxy amines 17a–c (Scheme 4). The conversion of amines 17a–c to the sulfonamides 18a–c was realized by coupling the amines with

Scheme 5. Synthesis of Macrocyclic Inhibitors 20a–c, 21a–c, and 22a–c

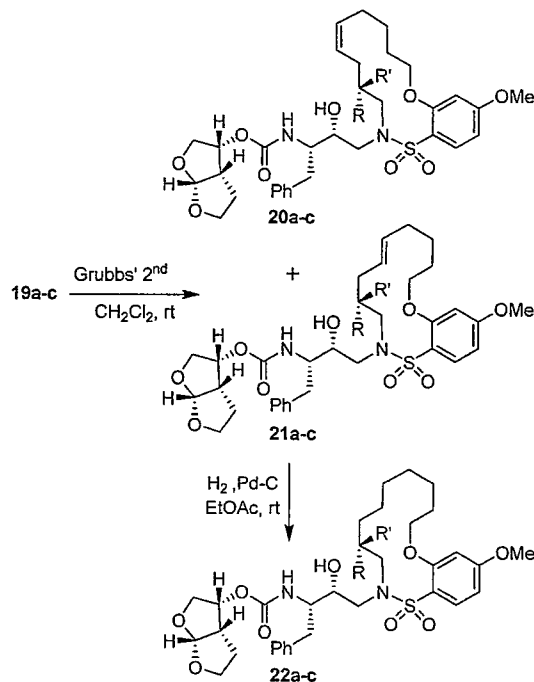


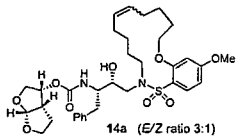
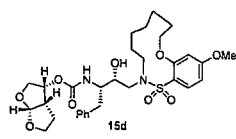
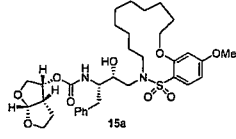
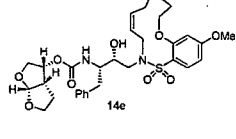
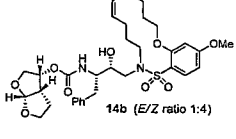
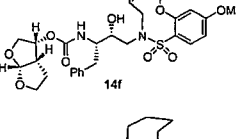
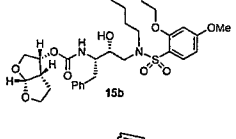
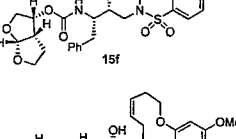
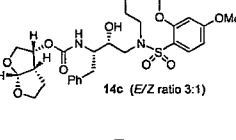
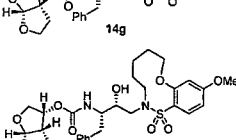
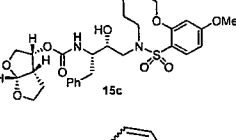
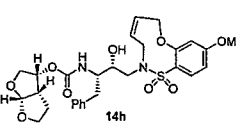
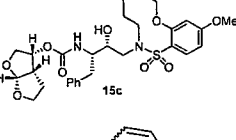
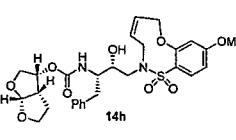
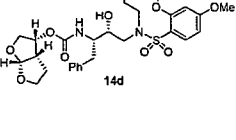
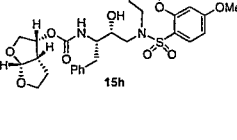
Table 1. Enzyme Inhibitory and Antiviral Activity of Inhibitors 13a–h

compd	m	n	K _i (nM)	IC ₅₀ (nM) ^a	ring size by RCM
13a	4	4	16.5 ± 0.5	> 1000	15
13b	4	3	11.5 ± 0.4	> 1000	14
13c	4	2	6.9 ± 0.1	ND	13
13d	4	1	10 ± 2	ND	12
13e	1	4	1.70 ± 0.07	270	12
13f	1	3	1.02 ± 0.08	290	11
13g	1	2	0.63 ± 0.01	ND	10
13h	1	1	0.10 ± 0.01	ND	9

^aHuman T-lymphoid cells, MT-2 cells (2×10^3), were exposed to HIV-1_{LA1} (100 TCID₅₀), cultured in the presence of each PI, and IC₅₀ values were determined by using the MTT assay. The IC₅₀ values of saquinavir (SQV) and amprenavir (APV) tested as reference agents were 16 and 27 nM, respectively. ND: not determined.

sulfonyl chloride 7d in the presence of pyridine. Removal of the Boc protecting group from sulfonamides 18a–c using 30% trifluoroacetic acid in CH₂Cl₂ furnished the corresponding amines, which were then coupled with the mixed carbonate of activated bis-THF¹⁵ (12) to give acyclic inhibitors 19a–c. A ring closing metathesis reaction using Grubbs' second-generation catalyst¹⁶ (Scheme 5) provided a *E/Z* mixture of unsaturated macrocyclic inhibitors 20a–c and 21a–c, which were separated by reverse-phase HPLC and identified by 2-D NMR (COSY and NOESY). The unsaturated compounds

Table 2. Enzyme Inhibitory and Antiviral Activity of Inhibitors 14a–h and 15a–h

Ring size	Inhibitor structure	K_i (nM)	IC_{50} (nM) ^a	Ring size	Inhibitor structure	K_i (nM)	IC_{50} (nM) ^a
15	 14a (E/Z ratio 3:1)	0.38 ± 0.03	120	12	 15d	0.017 ± 0.001	14
15	 15a	0.82 ± 0.03	318	12	 14e	0.08 ± 0.02	23
14	 14b (E/Z ratio 1:4)	0.082 ± 0.008	4	11	 14f	0.077 ± 0.004	20
14	 15b	0.67 ± 0.02	49	11	 15f	0.15 ± 0.01	95
13	 14c (E/Z ratio 3:1)	0.045 ± 0.005	2	10	 14g	0.051 ± 0.004	15
13	 15c	0.47 ± 0.002	22	10	 15g	0.09 ± 0.01	5.5
13	 15c	0.47 ± 0.002	22	9	 14h	2.4 ± 0.3	n.t. ^b
12	 14d	0.058 ± 0.005	14	9	 15h	1.27 ± 0.03	77

^aMT-2 human T-lymphoid cells exposed to HIV-1_{LAI}; saquinavir and amprenavir exhibited IC_{50} values of 16 and 27 nM, respectively. ^bn.t. = not tested.

20a–c and 21a–c were subsequently hydrogenated over 10% Pd–C as the catalyst to yield inhibitors 22a–c.

Biological Evaluation and Discussion

The inhibitory potencies of acyclic and cyclic inhibitors were measured by the assay protocol of Toth and Marshall.¹⁷ Compounds that showed potent enzyme inhibition K_i values were further evaluated in an antiviral assay. Biological results for the acyclic compounds 13a–h are shown in Table 1. In general, elongation of the carbon chains resulted in lower enzyme inhibitory activity. Extension of the β -hydroxyl amine chain by three methylene groups resulted in a 10-fold loss in activity (13a K_i = 16 nM versus 13e K_i = 1.7 nM). Similarly, extension of the ether carbon chain by three methylene groups resulted in a 17-fold loss in activity (13h K_i = 0.10 nM versus 13e K_i = 1.7 nM).

Interestingly, conversion of these acyclic inhibitors 13a–h to their cyclic analogues 14a–h and 15a–h resulted in significant improvements of enzyme inhibitory and antiviral activity as shown in Table 2. For example, the 14-membered macrocyclic inhibitors 14b and 15b have K_i values of less than 0.7 nM and IC_{50} values less than 49 nM, whereas their corresponding acyclic inhibitor 13b had a K_i of 11 nM and IC_{50} value of > 1000 nM (greater than 15-fold and 20-fold change, respectively). Another trend observed is a preference of the S1'-subsite for macrocyclic rings of size 10 and 13. This preference is consistent with our energy-minimized model structure of a saturated 13-membered prototype inhibitor 15c where a macrocycle is incorporated in place of the P1'-isobutyl group and attached at the ortho-position of the sulfonamide ring of inhibitor 2 as shown in Figure 2. The model of inhibitor 15c was created based upon the crystal structure of inhibitor 2-bound HIV-1 protease.

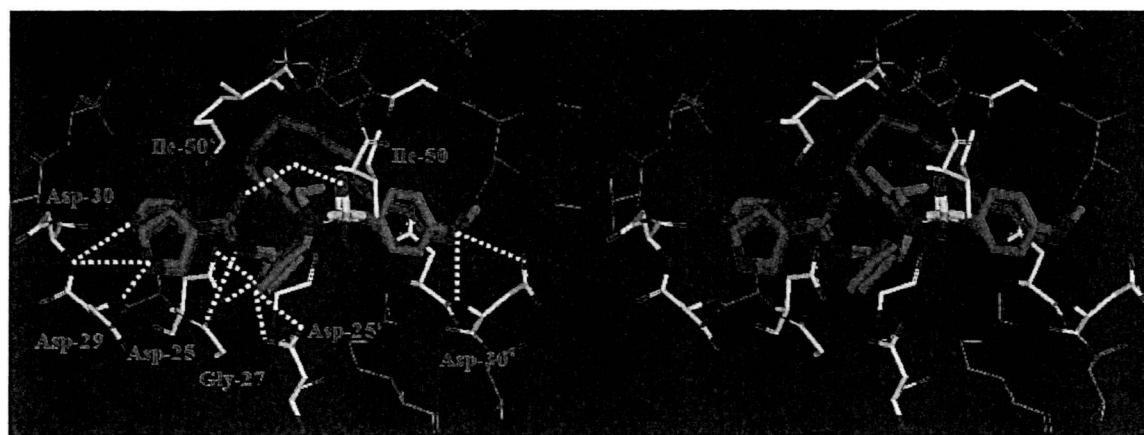
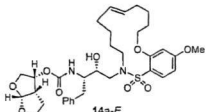
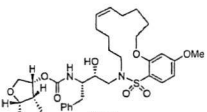
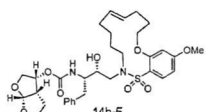
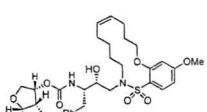
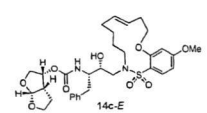
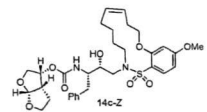


Figure 2. An overlay of energy-minimized macrocyclic inhibitor **15c** (magenta) with the X-ray structure of inhibitor **2** (green)-bound HIV-1 protease.

Table 3. Enzyme Inhibitory and Antiviral Activity of *E* and *Z* Isomers of **14a–c**

Ring size	Inhibitor structure	K_i (nM)	IC_{50} (nM) ^a
15		0.24 ± 0.07	360
15		0.16 ± 0.04	>1000
14		0.18 ± 0.01	6.6
14		0.9 ± 0.3	2.9
13		0.06 ± 0.01	7
13		0.012 ± 0.004	4.6

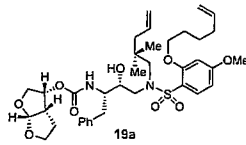
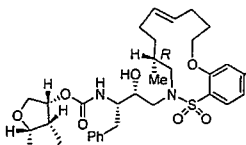
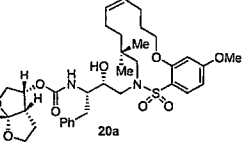
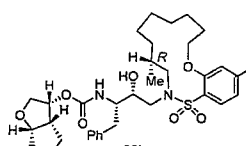
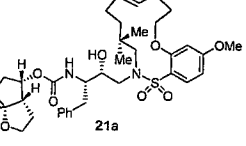
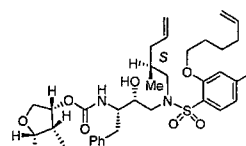
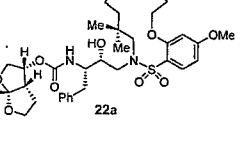
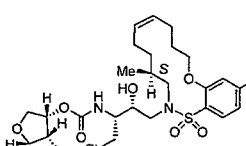
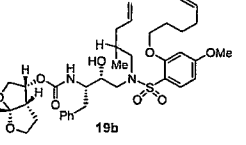
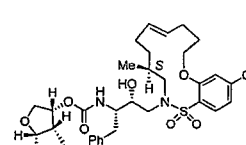
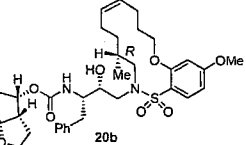
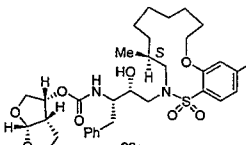
^aMT-2 human T-lymphoid cells exposed to HIV-1_{LAI}; saquinavir and amprevir exhibited IC_{50} values of 16 and 27 nM, respectively.

Indeed, the most potent compound of the series, inhibitor **14c** incorporating a 13-membered ring, showed a K_i of 45 pM and IC_{50} of 2 nM. It would appear the 13-membered ring provides an optimally sized macrocyclic ring as increasing the ring size to 14 or 15 as well as decreasing the ring to 12 or 11 resulted in reduced enzymatic inhibitory and antiviral activity. Interestingly, inhibitors incorporating a 10-membered ring (**14g** and **15g**) were also exceedingly potent, displaying a similar activity profile as the 13-membered ring **14c** (**14g** K_i = 51 pM; **15g** K_i = 86 pM and IC_{50} = 5.5 nM).

In comparing the potency of **14c** to its unsaturated analogue **15c**, we observed a dramatic improvement in the K_i and IC_{50} values for the unsaturated cyclic inhibitor **14c**. Furthermore, the effect appeared to remain consistent throughout the variously sized unsaturated macrocycles **14a–h** as compared to their saturated analogues **15a–h**. For the 13-membered ring series, the presence of a double bond resulted in a 10-fold increase in both K_i and IC_{50} values (**14c** K_i = 45 pM and IC_{50} = 2 nM as compared to **15c** K_i = 470 pM and IC_{50} = 22 nM). Similar differences in potency can be seen for the 11, 14, and 15-membered macrocycles, although for the smaller rings 9, 10, and 12, the effect is less pronounced. This effect may be explained by a restriction of conformation in the molecule that results from the presence of the double bond and leads to a better fit in the hydrophobic pocket of the S1'-subsite. These observations led us to take a closer look at the olefinic compounds and evaluate the importance of the stereochemistry of this group. As shown in Table 3, only minor variations in activity (less than 5-fold) were observed between the *E* and *Z* isomers of the 13, 14, and 15-membered macrocycles. For the 13-membered ring system, the *Z* isomer was favored over the *E* configuration.

On the basis of these exciting results for this series of macrocyclic inhibitors, we began to envision possible substitutions that could be made across the macrocyclic ring system in order to further enhance biological activity. The energy-minimized structure of **15b**-bound HIV-1 protease with **2**-bound HIV-1 protease (Figure 2) suggested that a single methyl substitution β to the macrocyclic amine could fill an additional hydrophobic pocket previously filled by darunavir's isobutyl group. To this end, we designed and synthesized a series of mono- and dimethylated 14-membered macrocyclic ring systems and evaluated the impact of this substitution on the biological activity. Geminal dimethyl at this location (**19a** through **22a**, Table 4) significantly decreased (10-fold) the enzyme inhibition and greatly reduced antiviral activity. In most cases, the addition of a single methyl group to the ring also reduced biological activity as compared to **14b** and **15b** although results varied greatly depending upon the stereochemistry of the ring systems. Inhibitors **20c** and **21b** were the most potent compounds from this series with K_i = 0.31 and 2.8 nM and IC_{50} = 9.0 and 6.3 nM, respectively. In general, antiviral potency of cyclic inhibitors was superior to that of their acyclic homologues, unsaturated macrocyclic derivatives

Table 4. Enzyme Inhibitory Activity of 19a–c, 20a–c, and 21a–c

Inhibitor structure	K_i (nM)	IC_{50} (nM) ^a	Inhibitor structure	K_i (nM)	IC_{50} (nM) ^a
	82 ± 2	>1000		2.8 ± 0.3	6.3
	16 ± 1	>1000		3.7 ± 0.3	650
	6.9 ± 0.2	>1000		58 ± 6	>1000
	6.8 ± 0.8	>1000		0.31 ± 0.03	9
	15 ± 3	380		0.15 ± 0.01	52
	6 ± 1	200		0.07 ± 0.02	170

^a MT-2 human T-lymphoid cells exposed to HIV-1_{LAI}; saquinavir and amprenavir exhibited IC_{50} values of 16 and 27 nM, respectively.

were more potent than the corresponding saturated derivatives, and the addition of methyl substituents tended to decrease potency. The two most potent macrocyclic inhibitors identified were **14c** and **14b** having enzyme inhibitory K_i values of 45 and 82 pM and antiviral IC_{50} values of 2 and 4 nM, respectively.

The inhibitors **14b** and **14c** were then examined for their activity against a clinical wild-type X₄-HIV-1 isolate (HIV-1_{ERS104pre}) along with various multidrug-resistant clinical X₄- and R₅-HIV-1 isolates using PBMCs as target cells.^{6b} The results are shown in Table 5. As can be seen, the potency of inhibitors **14b** and **14c** against HIV-1_{ERS104pre} (IC_{50} = 7 and 5 nM, respectively) are superior to FDA approved inhibitors IDV, APV, and LPV. It is comparable to saquinavir but nearly 2-fold less potent than darunavir (IC_{50} = 3 nM).^{6b} In these studies, both indinavir and lopinavir were unable to suppress the replication of the multidrug-resistant clinical isolates examined that include HIV-1_{MDR/B}, HIV-1_{MDR/C}, HIV-1_{MDR/TM}, HIV-1_{MRR/MM}, and HIV-1_{MDR/JSL}. Of particular note, lopinavir which is widely used as a first-line

agent in HAART treatment regimens, was not active against these multidrug-resistant clinical isolates. Amprenavir displayed a 10-fold or greater reduction in potency except against HIV-1_{MDR/MM}, where it showed a 7-fold reduction in potency. Inhibitor **14c**, while less potent than darunavir, maintained 7-fold or better potency over amprenavir against HIV-1_{MDR/C}, HIV-1_{MDR/G}, HIV-1_{MDR/TM}, and HIV-1_{MDR/JSL}. It maintained over a 6-fold potency against HIV-1_{MDR/MM}. Inhibitor **14b** maintained superior potency against HIV-1_{MDR/C} and HIV-1_{MDR/G} (greater than 12- and 21-fold) compared to amprenavir. It maintained 3-fold or better potency compared to amprenavir against all other multidrug-resistant clinical isolates tested. Both inhibitors **14b** and **14c** have shown low cytotoxicity (CC_{50} values 49 and 33 μ M, respectively) in target CD₄⁺ MT-2 cells. Furthermore, they prevented the replication of HIV-1_{NL4-3} variants selected against up to 5 μ M of saquinavir, lopinavir, and indinavir with IC_{50} values of 20–46 nM. More detailed virologic studies with inhibitors **14c** and **14b** will be published in due course.

Table 5. Antiviral Activity of Macrocyclic Inhibitors against Multidrug Resistant Clinical Isolates in PHA-PBMs^a

virus	SQV	IDV	APV	LPV	DRV	14b	14c
HIV-1 _{ERS104pre} (wild-type: X4)	0.008 ± 0.005	0.043 ± 0.004	0.030 ± 0.005	0.034 ± 0.002	0.003 ± 0.0002	0.007 ± 0.002	0.005 ± 0.003
HIV-1 _{MDR/B} (X4)	0.27 ± 0.073 (34)	> 1 (> 23)	> 1 (> 33)	> 1 (> 29)	0.019 ± 0.012 (6)	0.089 ± 0.016 (13)	0.037 ± 0.016 (7)
HIV-1 _{MDR/C} (X4)	0.032 ± 0.002 (11)	> 1 (> 23)	0.37 ± 0.011 (12)	> 1 (> 29)	0.008 ± 0.006 (3)	0.029 ± 0.001 (4)	0.044 ± 0.002 (9)
HIV-1 _{MDR/G} (X4)	0.030 ± 0.002 (4)	0.34 ± 0.14 (5)	0.43 ± 0.004 (14)	0.26 ± 0.04 (8)	0.023 ± 0.006 (5)	0.028 ± 0.004 (4)	0.057 ± 0.012 (11)
HIV-1 _{MDR/TM} (X4)	0.26 ± 0.04 (33)	> 1 (> 23)	0.32 ± 0.007 (11)	> 1 (> 29)	0.004 ± 0.001 (1)	0.072 ± 0.014 (10)	0.027 ± 0.001 (6)
HIV-1 _{MDR/MM} (R5)	0.19 ± 0.05 (24)	> 1 (> 23)	0.21 ± 0.222 (7)	> 1 (> 29)	0.011 ± 0.002 (4)	0.055 ± 0.025 (8)	0.033 ± 0.010 (7)
HIV-1 _{MDR/JSL} (R5)	0.30 ± 0.02 (37)	> 1 (> 23)	0.62 ± 0.02 (21)	> 1 (> 29)	0.027 ± 0.011 (9)	0.21 ± 0.032 (30)	0.073 ± 0.07 (15)

^a Amino acid substitutions identified in the protease-encoding region compared to the consensus type B sequence cited from the Los Alamos database include L63P in HIV-1_{ERS104pre}; L10I, K14R, L33I, M36I, M46I, F53I, K55R, I62 V, L63P, A71 V, G73S, V82A, L90M, and I93L in HIV-1_{MDR/B}; L10I, I15 V, K20R, L24I, M36I, M46L, I54 V, I62 V, L63P, K70Q, V82A, and L89 M in HIV-1_{MDR/C}; L10I, V11I, T12E, I15 V, L19I, R41K, M46L, L63P, A71T, V82A, and L90 M in HIV-1_{MDR/G}; L10I, K14R, R41K, M46L, I54 V, L63P, A71 V, V82A, L90M, and I93L in HIV-1_{MDR/TM}; L10I, K43T, M46L, I54 V, L63P, A71 V, V82A, L90M, and Q92K in HIV-1_{MDR/MM}; L10I, L24I, I33F, E35D, M36I, N37S, M46L, I54 V, R57K, I62 V, L63P, A71 V, G73S, and V82A in HIV-1_{MDR/JSL}. HIV-1_{ERS104pre} served as a source of wild-type HIV-1. IC₅₀ values were determined by using PHA-PBMs as target cells, and inhibition of p24 Gag protein production by each drug was used as an end point. Numbers in parentheses represent *n*-fold changes of IC₅₀ values for each isolate compared to IC₅₀ values for wild-type HIV-1_{ERS104pre}. All assays were conducted in duplicate or triplicate, and data shown represent mean values (± standard deviation) derived from results of three independent experiments.

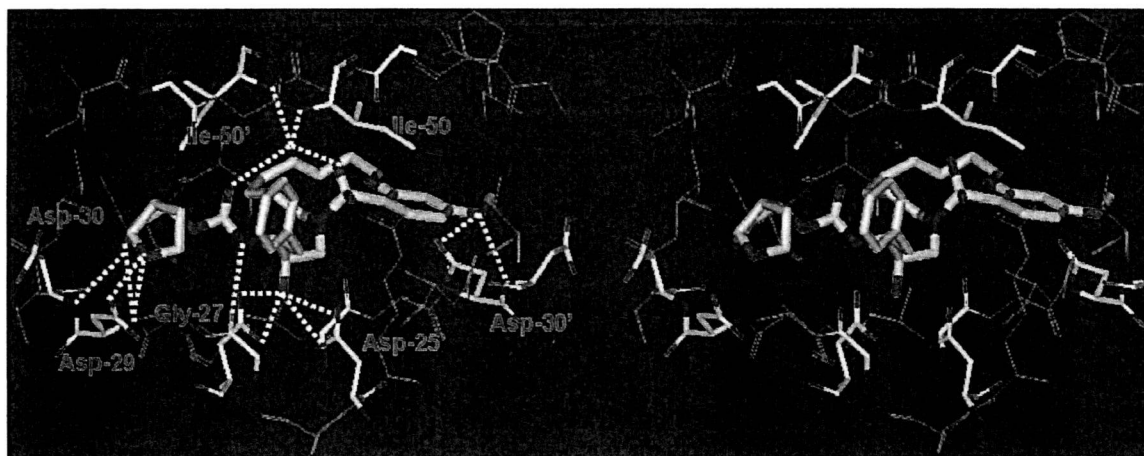


Figure 3. A stereoview of the X-ray structure of macrocyclic inhibitor **14c** (light gray)-bound HIV-1 protease. All strong hydrogen bonding interactions are shown as dotted lines.

The reason why these macrocyclic inhibitors maintained impressive potency against multidrug-resistant clinical isolates is possibly due to their ability to make extensive hydrogen bonds with protease backbone and effectively fill in the hydrophobic pockets in the S1'–S2'-subsites.

X-ray Crystallography

To gain molecular insights into ligand-binding site interactions responsible for the potent antiviral activity of inhibitor **14c**, we have determined an X-ray crystal structure of the inhibitor complexed with wild-type protease. The crystal structure was solved and refined at 1.17 Å resolution with an *R*-factor and *R*_{free} of 16.0% and 19.4%, respectively. In this high resolution structure, the inhibitor **14c** was bound to the HIV-1 protease active site in the two orientations with a ratio of 1:1. A stereoview of the X-ray structure of **14c**-bound HIV-1 protease is shown in Figure 3. As can be seen, the inhibitor makes extensive interactions involving the P2 to P2'-ligands in the protease active site, most notably through favorable polar interactions including hydrogen bonds and weaker C–H···O interactions in the active site. The transition-state hydroxyl group in **14c** forms asymmetric hydrogen bonding interactions with all four carboxylate oxygen atoms of the Asp25 and Asp25' with distances of 2.5–3.3 Å. The conserved tetrahedral water molecule forms hydrogen bonds with one of

the sulfonamide oxygens, the urethane carbonyl oxygen, and the backbone amide of Ile50 and Ile50' with distances of 2.6–3.1 Å. These interactions have been observed in a majority of HIV-1 protease complexes with the inhibitors¹⁸ and substrate analogues.¹⁹ The flexible P1'–P2' macrocyclic ligand nicely packs into the hydrophobic pocket in the S1'-subsite. It also makes weaker C–H···O interactions, which play important roles as we have reported earlier.^{20–22} The macrocyclic ring zigzags into a crown shape and fits well in between the S1' and S2'-pockets. The protein–ligand complex shows three major interactions with the carbonyl oxygen of backbone residues, one with Gly27' and two with Gly48', with distances ranging from 3.0 to 3.6 Å. In comparison to the X-ray structures of the protease with **1** and **2**, the P1-phenyl ring in **14c** is rotated about 30° toward Asp 29' along the backbone. The macrocycle acts more or less like a spring that pushes against the P1-phenyl ring, causing this rotation.

Both P2 and P2' ligands form five strong N–H···O hydrogen bonds with the protease backbone. Of these, three hydrogen bonds are formed between the P2-bis-THF ring oxygens and the backbone amide nitrogens of Asp29 and Asp30 with distances of 3.1, 3.0, and 3.2 Å. The fourth interaction is between the P2-urethane NH and the carbonyl oxygen of Gly27 with a distance of 3.0 Å. The fifth backbone interaction is between the *p*-methoxy group of the P2'-sulfonamide and the

amide nitrogen of Asp30', with a distance of 3.0 Å. All of these ligand–backbone interactions are present in the X-ray structure of 2-bound HIV-1 protease as well. This backbone binding with the main chain atoms of the protease may be responsible for both inhibitors' (2 and 14c) abilities to maintain robust potency against multidrug-resistant HIV-1 variants.

Conclusions

In summary, we have designed novel macrocyclic protease inhibitors modifying P1'–P2' ligands of darunavir-like PIs and investigated their biological activity. The inhibitors were designed to maintain key hydrogen bonding interactions with protease backbone, similar to darunavir. The design of macrocycles involving the P1'–P2'-ligands is based upon the premise that a flexible macrocycle would effectively repack the hydrophobic pocket in the S1' to S2'-subsites when it is altered by mutations. We have investigated inhibitors containing 9–15-membered macrocycles containing both *E/Z* olefins and the corresponding saturated derivatives. Grubbs' metathesis reaction was the key step in building these inhibitors in very good yields. Most remarkably, all macrocyclic inhibitors are significantly more potent than their acyclic counterparts. The saturated inhibitors are in general less active than the corresponding unsaturated derivatives. Our investigation resulted in the identification of inhibitors 14b and 14c, which have displayed significantly better antiviral activity than many of the currently FDA-approved inhibitors. Inhibitor 14b contains a 14-membered ring with a *Z*-olefin, and 14c contains a 13-membered ring with an *E*-olefin. Both inhibitors exerted potent activity against HIV-1_{LAI}, with IC₅₀ values of 4 and 2 nM, respectively. They have maintained excellent potency against multidrug-resistant HIV-1 variants. These inhibitors have shown low cytotoxicity (CC₅₀ values 49 and 33 μM, respectively) in target CD₄⁺ MT-2 cells. Furthermore, both inhibitors 14b and 14c blocked the replication of HIV-1_{NL4-3} variants, selected after exposure of up to 5 μM of saquinavir, lopinavir, and indinavir, with IC₅₀ values of 20–46 nM. The protein–ligand X-ray structure of 14c showed critical ligand-binding site interactions in the protease active site. Particularly, it maintained all key backbone hydrogen bonding interactions similar to darunavir and inhibitor 2. Also, the conformational flexibility of the P1'–P2' macrocycle most likely contributed to its impressive activity against multidrug-resistant clinical variants. Further design and optimization of P1'–P2' macrocyclic ligands are in progress.

Experimental Section

General Experimental Methods. Chemicals and reagents were purchased from commercial suppliers and used without further purification. Anhydrous solvents were obtained as follows: pyridine and dichloromethane were distilled from calcium hydride; tetrahydrofuran and diethyl ether were distilled from sodium with benzophenone as an indicator. All other solvents were reagent grade. All moisture sensitive reactions were carried out in oven-dried glassware under argon. ¹H NMR and ¹³C NMR spectra were recorded on a Bruker Avance ARX-400, Bruker DRX-500, or Bruker Avance-III-800 spectrometer. Chemical shifts are given in ppm and are referenced against the diluting solvent. For chloroform-*d*: ¹³C triplet = 77.00 CDCl₃ and ¹H singlet = 7.26 ppm. For methanol-*d*₄: ¹³C septuplet = 49.05 and ¹H quintuplet = 3.31 ppm. Characteristic splitting patterns due to spin–spin coupling are expressed as follows: br = broad, s = singlet, d = doublet, t = triplet, q = quartet, m = multiplet, sept = septuplet. All coupling constants are measured in hertz. FTIR spectra were recorded on a Mattson Genesis II

FT-IR spectrometer or a Perkin-Elmer spectrometer L1185247 using a NaCl plate or KBr pellet. Optical rotations were recorded on a Perkin-Elmer 341 or Rudolph Research Autopol III polarimeter. Low resolution mass spectra were recorded on a FinniganMAT LCQ or Hewlett-Packard Engine mass spectrometer. High-resolution mass spectra were recorded on a FinniganMAT XL95 mass spectrometer calibrated against PPG. Column chromatography was performed with Whatman 240–400 mesh silica gel under low pressure of 3–5 psi. TLC was carried out with E. Merck silica gel 60-F-254 plates. HPLC data was collected using a system composed of an Agilent 1100 series degasser, quaternary pump, thermostatable column compartment, variable wavelength detector, and Agilent 1200 series autosampler and fraction collector controlled by Chemstation software. All chromatographic reagents used were HPLC grade. The reported inhibitors were found to be >95% pure by reversed-phase gradient HPLC (see Supporting Information for specific method conditions).

1-(Hex-5-enyloxy)-3-methoxybenzene (5a). To a stirred solution of 3-methoxy phenol (1.24 g, 10 mmol), 5-hexen-1-ol, 4a (1.4 mL, 12 mmol), and Ph₃P (3.14 g, 12 mmol) in THF (20 mL) at 0 °C was added DIAD (2.3 mL, 12 mmol) dropwise. After stirring the solution for 30 min at 0 °C, the reaction mixture was warmed to 23 °C and stirred for 3 h. The reaction mixture was concentrated in vacuo, and the residue was subjected to column chromatography (98:2 hexanes:EtOAc) to yield 5a (1.98 g, 96% yield) as a colorless oil. ¹H NMR (400 MHz, CDCl₃) δ 1.58–1.66 (m, 2H), 1.80–1.88 (m, 2H), 2.15–2.20 (m, 2H), 3.82 (s, 3H), 3.98 (t, *J* = 6.4 Hz, 2H), 5.02–5.12 (m, 2H), 5.83–5.92 (m, 1H), 6.52–6.56 (m, 3H), 7.19–7.24 (m, 1H). ¹³C NMR (100 MHz, CDCl₃) δ 25.3, 28.7, 33.4, 55.1, 67.6, 100.9, 106.0, 106.6, 114.7, 129.8, 138.5, 160.3, 160.8. FT-IR (film, NaCl) ν_{max} = 3075, 2939, 1599, 1493, 1287, 1200, 1152, 1046 cm⁻¹. CI LRMS (*m/z*): 207.25 [M + H]⁺.

1-Methoxy-3-(pent-4-enyloxy)benzene (5b). Title compound was obtained from 4-penten-1-ol 4b, as described for 5a in 95% yield after flash-chromatography (98:2 hexanes:EtOAc) as a colorless oil. ¹H NMR (400 MHz, CDCl₃) δ 1.88–1.94 (m, 2H), 2.25–2.30 (m, 2H), 3.81 (s, 3H), 3.98 (t, *J* = 6.4 Hz, 2H), 5.03–5.13 (m, 2H), 5.85–5.95 (m, 1H), 6.51–6.56 (m, 3H), 7.20 (t, *J* = 8.1 Hz, 1H). ¹³C NMR (100 MHz, CDCl₃) δ 28.3, 30.0, 55.1, 67.0, 100.9, 106.0, 106.6, 115.1, 129.7, 137.7, 160.2, 160.7. FT-IR (film, NaCl) ν_{max} = 3076, 2940, 1599, 1492, 1287, 1200, 1152, 1048 cm⁻¹. CI LRMS (*m/z*): 193.25 [M + H]⁺.

1-(But-3-enyloxy)-3-methoxybenzene (5c). Title compound was obtained from 3-buten-1-ol 4c, as described for 5a in 96% yield after flash-chromatography (98:2 hexanes:EtOAc) as a colorless oil. ¹H NMR (400 MHz, CDCl₃) δ 2.54–2.60 (m, 2H), 3.81 (s, 3H), 4.02 (t, *J* = 6.7 Hz, 2H), 5.13–5.23 (m, 2H), 5.89–5.97 (m, 1H), 6.51–6.56 (m, 3H), 7.20 (t, *J* = 8.1 Hz, 1H). ¹³C NMR (100 MHz, CDCl₃) δ 33.6, 55.1, 67.1, 100.9, 106.2, 106.6, 116.9, 129.8, 134.4, 160.1, 160.8. FT-IR (film, NaCl) ν_{max} = 3136, 2378, 1644, 1509 cm⁻¹. CI LRMS (*m/z*): 179.20 [M + H]⁺.

1-(Allyloxy)-3-methoxybenzene (5d). Title compound was obtained from allyl alcohol 4d as described for 5a in 96% yield after flash-chromatography (98:2 hexanes:EtOAc) as a colorless oil. ¹H NMR (400 MHz, CDCl₃) δ 3.81 (s, 3H), 4.02 (d, *J* = 6.7 Hz, 2H), 5.13–5.23 (m, 2H), 5.89–5.97 (m, 1H), 6.51–6.56 (m, 3H), 7.20 (t, *J* = 8.1 Hz, 1H). ¹³C NMR (100 MHz, CDCl₃) δ 55.1, 67.1, 100.9, 106.2, 106.6, 116.9, 129.8, 134.4, 160.1, 160.8.

2-(Hex-5-enyloxy)-4-methoxybenzenesulfonic Acid (6a). To 6a (2 g, 9.7 mmol) was added acetic anhydride (1.4 mL, 14.5 mmol), and the resulting mixture was stirred at 0 °C. To this was then added concentrated H₂SO₄ (1.1 g) followed by methanol (20 mL). The resulting solution was warmed to 23 °C and stirred for 12 h. After this time, the reaction mixture was concentrated in vacuo and the resulting red oil was subjected to column chromatography (88:12 CH₂Cl₂:MeOH) to give 6a (1.06 g, 38%) as a red waxy solid. ¹H NMR (400 MHz, D₂O) δ 1.44

(quintet, $J=7.4$ Hz, 2H), 1.66–1.73 (m, 2H), 1.99 (q, $J=7.1$ Hz, 2H), 3.70 (s, 3H), 3.98 (t, $J=6.5$ Hz, 2H), 4.85–4.97 (m, 2H), 5.74–5.92 (m, 1H), 6.52–6.56 (m, 2H), 7.19–7.24 (m, 1H). ^{13}C NMR (100 MHz, D_2O) δ 25.3, 28.7, 33.4, 55.1, 67.6, 100.9, 106.0, 106.6, 114.7, 129.8, 138.5, 160.3, 160.8. ESI (m/z): 285.09 [$\text{M} - \text{H}$] $^-$.

4-Methoxy-2-(pent-4-enyloxy)benzenesulfonic Acid (6b). Title compound was obtained from ether **5b** as described for **6a** in 36% yield after flash-chromatography (88:12 CH_2Cl_2 :MeOH) as a white solid. ^1H NMR (400 MHz, D_2O) δ 1.75–1.82 (m, 2H), 2.10–2.16 (m, 2H), 3.69 (s, 3H), 3.98 (t, $J=6.4$ Hz, 2H), 4.88–5.00 (m, 2H), 5.77–5.87 (m, 1H), 6.45 (dd, $J=8.6$, 2.2 Hz, 1H), 6.51 (d, $J=2.1$ Hz, 1H), 7.58 (d, $J=8.8$ Hz, 1H). ^{13}C NMR (100 MHz, D_2O) δ 28.0, 29.9, 56.1, 68.7, 100.5, 104.9, 115.5, 123.7, 130.2, 139.4, 157.8, 163.5. ESI (m/z): 271.07 [$\text{M} - \text{H}$] $^-$.

2-(But-3-enyloxy)-4-methoxybenzenesulfonic Acid (6c). Title compound was obtained from ether **5c** as described for **6a** in 30% yield after flash-chromatography (88:12 CH_2Cl_2 :MeOH) as a white solid. ^1H NMR (400 MHz, D_2O) δ 2.38–2.43 (m, 2H), 3.62 (s, 3H), 3.98 (t, $J=6.8$ Hz, 2H), 4.93–5.05 (m, 2H), 5.77–5.87 (m, 1H), 6.37 (dd, $J=8.6$, 2.2 Hz, 1H), 6.43 (d, $J=2.4$ Hz, 1H), 7.58 (d, $J=8.8$ Hz, 1H). ^{13}C NMR (100 MHz, D_2O) δ 33.3, 56.1, 68.8, 100.6, 105.0, 117.5, 123.7, 130.2, 135.4, 157.5, 163.4. ESI (m/z): 257.10 [$\text{M} - \text{H}$] $^-$.

2-(Allyloxy)-4-methoxybenzenesulfonic Acid (6d). Title compound was obtained from ether **5d** as described for **6a** in 35% yield after flash-chromatography (88:12 CH_2Cl_2 :MeOH) as a white solid. ^1H NMR (400 MHz, D_2O) δ 3.71 (s, 3H), 4.58–4.75 (m, 2H), 5.16–5.38 (m, 2H), 5.92–5.99 (m, 1H), 6.47–6.57 (m, 2H), 7.58 (d, $J=8.8$ Hz, 1H). ^{13}C NMR (100 MHz, D_2O) δ 56.1, 69.7, 101.1, 105.3, 118.0, 123.7, 130.6, 133.2, 157.1, 163.5. ESI (m/z): 243.13 [$\text{M} - \text{H}$] $^-$.

2-(Hex-5-enyloxy)-4-methoxybenzene-1-sulfonyl Chloride (7a). To a stirring solution of sulfonic acid **6a** (266 mg, 0.9 mmol) in pyridine (2 mL) was added thionyl chloride (0.2 mL, 2.8 mmol) dropwise. The resulting solution was allowed to stir for 4 h and then the reaction mixture concentrated in vacuo. The resulting residue was purified using column chromatography (5:1 hexanes:EtOAc) to give **7a** (140 mg, 50%) as a colorless oil. ^1H NMR (400 MHz, CDCl_3) δ 1.63–1.70 (m, 2H), 1.87–1.93 (m, 2H), 2.10–2.16 (m, 2H), 3.88 (s, 3H), 4.14 (t, $J=6.2$ Hz, 2H), 4.95–5.05 (m, 2H), 5.76–5.86 (m, 1H), 6.51–6.54 (m, 2H), 7.84 (d, $J=9.6$ Hz, 1H). ^{13}C NMR (100 MHz, CDCl_3) δ 24.9, 28.1, 33.1, 55.9, 69.2, 99.9, 104.6, 114.7, 124.3, 131.7, 138.3, 158.7, 166.8.

4-Methoxy-2-(pent-4-enyloxy)benzene-1-sulfonyl Chloride (7b). Title compound was obtained from ether **6b** as described for **7a** in 48% yield after flash-chromatography (6:1 hexanes:EtOAc) as a colorless oil. ^1H NMR (400 MHz, CDCl_3) δ 1.96–1.2.03 (m, 2H), 2.31–2.37 (m, 2H), 3.88 (s, 3H), 4.15 (t, $J=6.2$ Hz, 2H), 4.99–5.09 (m, 2H), 5.79–5.90 (m, 1H), 6.51–6.54 (m, 2H), 7.84 (d, $J=9.2$ Hz, 1H). ^{13}C NMR (100 MHz, CDCl_3) δ 27.8, 29.7, 55.9, 68.4, 99.9, 104.6, 115.6, 124.3, 131.7, 137.3, 158.6, 166.8.

2-(But-3-enyloxy)-4-methoxybenzene-1-sulfonyl Chloride (7c). Title compound was obtained from ether **6c** as described for **7a** in 52% yield after flash-chromatography (6:1 hexanes:EtOAc) as a colorless oil. ^1H NMR (300 MHz, CDCl_3) δ 2.62–2.70 (m, 2H), 3.88 (s, 3H), 4.19 (t, $J=6.2$ Hz, 2H), 5.12–5.25 (m, 2H), 5.91–6.05 (m, 1H), 6.52–6.56 (m, 2H), 7.86 (d, $J=9.2$ Hz, 1H).

2-(Allyloxy)-4-methoxybenzene-1-sulfonyl Chloride (7d). Title compound was obtained from ether **6d** as described for **7a** in 58% yield after flash-chromatography (6:1 hexanes:EtOAc) as a colorless oil. ^1H NMR (400 MHz, CDCl_3) δ 3.88 (s, 3H), 4.72 (d, $J=4.4$ Hz, 2H), 5.33 (d, $J=10.6$ Hz, 1H), 5.57 (d, $J=17.3$ Hz, 1H), 5.99–6.07 (m, 1H), 6.52–6.55 (m, 2H), 7.83 (d, $J=8.7$ Hz, 1H). ^{13}C NMR (100 MHz, CDCl_3) δ 55.9, 69.7, 100.5, 105.0, 118.1, 124.4, 131.0, 131.7, 158.0, 166.7.

tert-Butyl (2*S*,3*R*)-4-(hex-5-enylamino)-3-hydroxy-1-phenylbutan-2-ylcarbamate (10a). A solution of hex-5-en-1-amine **9a** (297 mg, 3 mmol) and epoxide **8** (263 mg, 1 mmol) was heated to 60 °C in isopropyl alcohol (4 mL) for 4 h. The solvent was then

evaporated under reduced pressure, and the resulting residue was purified by silica chromatography (5:95 MeOH: CHCl_3) to give **10a** (350 mg, 97%) as a white solid. ^1H NMR (400 MHz, CDCl_3) δ 1.34 (s, 9H), 1.39–1.50 (m, 4H), 2.05 (q, $J=7$ Hz, 2H), 2.55–2.68 (m, 6H), 2.81–2.86 (m, 1H), 2.96 (dd, $J=4.5$, 14 Hz, 1H), 3.44–3.49 (m, 1H), 3.79 (br s, 1H), 4.72 (d, $J=8.7$ Hz, 1H), 4.92–5.02 (m, 2H), 5.74–5.84 (m, 1H), 7.17–7.28 (m, 5H). ^{13}C NMR (100 MHz, CDCl_3) δ 26.4, 28.2, 29.4, 33.4, 36.5, 49.6, 51.3, 54.1, 70.7, 79.3, 114.5, 126.2, 128.3, 129.4, 137.8, 138.6, 155.9. CI LRMS (m/z): 363.55 [$\text{M} + \text{H}$] $^+$.

tert-Butyl (2*S*,3*R*)-4-(allylamino)-3-hydroxy-1-phenylbutan-2-ylcarbamate (10b). Title compound was obtained from allylamine **9b** and epoxide **8** as described for **10a** in 99% yield after flash-chromatography (5:95 MeOH: CHCl_3) as a white solid. ^1H NMR (400 MHz, CDCl_3) δ 1.35 (s, 9H), 2.60–2.86 (m, 5H), 2.96 (dd, $J=4.5$, 14.1 Hz, 1H), 3.16–3.29 (m, 2H), 3.50–3.53 (m, 1H), 3.81 (br s, 1H), 4.73 (d, $J=9.1$ Hz, 1H), 5.10 (d, $J=10.3$ Hz, 1H), 5.17 (d, $J=17$ Hz, 1H), 5.81–5.91 (m, 1H), 7.13–7.32 (m, 5H). ^{13}C NMR (100 MHz, CDCl_3) δ 28.2, 36.5, 50.7, 52.1, 54.1, 70.9, 79.3, 116.2, 126.2, 128.3, 129.4, 136.3, 137.8, 155.9. CI LRMS (m/z): 321.50 [$\text{M} + \text{H}$] $^+$.

tert-Butyl-(2*S*,3*R*)-4-(*N*-(hex-5-enyl)-2-(hex-5-enyloxy)-4-ethoxyphenylsulfonamido)-3-hydroxy-1-phenylbutan-2-ylcarbamate (11a). To a stirring solution of **10a** (50 mg, 0.14 mmol) in pyridine (2 mL) was added **7a** (64 mg, 0.20 mmol), and the resulting solution was allowed to stir for 2 h at 23 °C. The reaction mixture was concentrated under reduced pressure, and the resulting residue was purified by flash column chromatography (3:1 hexanes:EtOAc) to yield **11a** (74 mg 84% yield) as a colorless oil. $[\alpha]_{\text{D}}^{20} -1.4$ (c 1.00, CHCl_3). ^1H NMR (400 MHz, CDCl_3) δ 1.25–1.34 (m, 11 H), 1.47–1.50 (m, 2H), 1.57–1.60 (m, 2H), 1.82–1.90 (m, 2H), 1.97 (q, $J=7.1$ Hz, 2H), 2.11 (q, $J=7.0$ Hz, 2H), 2.92–2.95 (m, 2H), 3.10–3.17 (m, 1H), 3.30 (br s, 3H), 3.76 (br s, 2H), 3.84 (s, 3H), 3.90–3.92 (m, 1H), 4.03 (t, $J=6.7$ Hz, 2H), 4.65 (d, $J=7.1$ Hz, 1H), 4.89–5.04 (m, 4H), 5.66–5.82 (m, 2H), 6.46 (d, $J=2$ Hz, 1H), 6.49 (dd, $J=8.8$, 2.3 Hz, 1H), 7.17–7.29 (m, 5H), 7.83 (d, $J=7.8$ Hz, 1H). ^{13}C NMR (100 MHz, CDCl_3) δ 24.9, 25.7, 27.9, 28.2, 28.3, 33.1, 33.2, 35.1, 49.9, 52.3, 54.5, 55.6, 69.1, 72.2, 79.4, 100.2, 104.1, 114.7, 115.0, 119.4, 126.2, 128.3, 129.5, 133.5, 137.8, 138.1, 138.2, 156.0, 157.6, 164.7. FT-IR (film, NaCl) ν_{max} = 3395, 2935, 1705, 1597, 1325 cm^{-1} . ESI (+) LRMS (m/z): 653.13 [$\text{M} + \text{Na}$] $^+$.

tert-Butyl-(2*S*,3*R*)-4-(*N*-(hex-5-enyl)-4-methoxy-2-(pent-4-enyloxy)phenylsulfonamido)-3-hydroxy-1-phenylbutan-2-ylcarbamate (11b). Title compound was obtained from **10a** and **7b**, as described for **11a** in 79% yield after flash-chromatography (3:1 hexanes:EtOAc) as a colorless oil. $[\alpha]_{\text{D}}^{20} -1.6$ (c 1.20, CHCl_3). ^1H NMR (400 MHz, CDCl_3) δ 1.25–1.37 (m, 12H), 1.43–1.51 (m, 2H), 1.88–1.98 (m, 4H), 2.27 (q, $J=7.1$ Hz, 2H), 2.86–2.97 (m, 2H), 3.10–3.17 (m, 1H), 3.25–3.31 (m, 3H), 3.76 (br s, 2H), 3.84 (s, 3H), 4.04 (t, $J=6.6$ Hz, 2H), 4.66 (d, $J=7.1$ Hz, 1H), 4.88–5.10 (m, 4H), 5.65–5.72 (m, 1H), 5.78–5.85 (m, 1H), 6.46 (d, $J=2$ Hz, 1H), 6.49 (dd, $J=8.8$, 2.0 Hz, 1H), 7.17–7.29 (m, 5H), 7.83 (d, $J=8.7$ Hz, 1H). ^{13}C NMR (100 MHz, CDCl_3) δ 25.7, 27.9, 28.2, 29.7, 33.1, 35.2, 49.8, 52.2, 54.6, 55.6, 68.4, 72.2, 79.4, 100.2, 104.1, 114.7, 115.7, 119.4, 126.2, 128.3, 129.5, 133.5, 137.0, 137.8, 138.2, 156.0, 157.6, 164.7. FT-IR (film, NaCl) ν_{max} = 3398, 2931, 1706, 1596, 1325 cm^{-1} . ESI (+) LRMS (m/z): 639.06 [$\text{M} + \text{Na}$] $^+$.

tert-Butyl-(2*S*,3*R*)-4-(2-(but-3-enyloxy)-*N*-(hex-5-enyl)-4-methoxyphenylsulfonamido)-3-hydroxy-1-phenylbutan-2-ylcarbamate (11c). Title compound was obtained from **10a** and **7c**, as described for **11a** in 50% yield after flash-chromatography (3:1 hexanes:EtOAc) as a colorless oil. $[\alpha]_{\text{D}}^{20} +0.6$ (c 2.00, CHCl_3). ^1H NMR (500 MHz, CDCl_3) δ 1.28–1.38 (m, 12H), 1.48–1.52 (m, 2H), 2.00 (q, $J=6.7$ Hz, 2H), 2.65 (q, $J=6.7$, 2H), 2.96 (br s, 2H), 3.14–3.18 (m, 1H), 3.30–3.39 (m, 3H), 3.79 (br s, 2H), 3.88 (s, 3H), 4.13 (t, $J=7.1$ Hz, 2H), 4.68 (d, $J=5.1$ Hz, 1H), 4.92–4.98 (m, 2H), 5.17–5.24 (m, 2H), 5.68–5.76 (m, 1H), 5.91–5.99 (m, 1H), 6.51 (d, $J=2$ Hz, 1H), 6.54 (dd, $J=8.8$, 2.0

Hz, 1H), 7.21–7.32 (m, 5H), 7.88 (d, $J = 8.8$ Hz, 1H). ^{13}C NMR (125 MHz, CDCl_3) δ 25.9, 28.2, 28.4, 29.9, 33.4, 35.4, 50.1, 52.5, 54.8, 55.9, 68.7, 72.5, 79.7, 100.6, 104.5, 114.9, 118.0, 119.8, 126.5, 128.6, 129.8, 133.7, 133.9, 138.1, 138.5, 156.3, 157.7, 165.0. FT-IR (film, NaCl) $\nu_{\text{max}} = 3394, 2931, 1704, 1596, 1325\text{ cm}^{-1}$. ESI (+) (m/z): 625.05 [$\text{M} + \text{Na}$] $^+$.

tert-Butyl-(2S,3R)-4-(2-(allyloxy)-N-(hex-5-enyl)-4-methoxyphenylsulfonamido)-3-hydroxy-1-phenylbutan-2-ylcarbamate (11d). Title compound was obtained from **10a** and **7d**, as described for **11a** in 64% yield after flash-chromatography (3:1 hexanes:EtOAc) as a colorless oil. $[\alpha]_{\text{D}}^{20} +1.1$ (c 2.80, CHCl_3). ^1H NMR (400 MHz, CDCl_3) δ 1.25–1.34 (m, 11H), 1.39–1.46 (m, 2H), 1.96 (q, $J = 7.0$ Hz, 2H), 2.89–2.96 (m, 2H), 3.08–3.15 (m, 1H), 3.24–3.30 (m, 3H), 3.77 (br s, 2H), 3.84 (s, 3H), 4.60 (d, $J = 5.4$ Hz, 2H), 4.66 (d, $J = 7.2$ Hz, 1H), 4.88–4.94 (m, 2H), 5.33 (d, $J = 10.4$, 2H), 5.43 (d, $J = 17.4$ Hz, 1H), 5.63–5.73 (m, 1H), 6.00–6.10 (m, 1H), 6.47 (d, $J = 1.8$ Hz, 1H), 6.54 (dd, $J = 8.9, 1.9$ Hz, 1H), 7.18–7.29 (m, 5H), 7.85 (d, $J = 8.8$ Hz, 1H). ^{13}C NMR (100 MHz, CDCl_3) δ 25.7, 27.8, 28.2, 33.1, 35.2, 49.9, 52.5, 54.5, 55.6, 69.9, 72.2, 79.4, 100.6, 104.4, 114.7, 119.4, 119.7, 126.2, 128.3, 129.5, 131.9, 133.5, 137.9, 138.2, 155.9, 157.0, 164.6. FT-IR (film, NaCl) $\nu_{\text{max}} = 3400, 2929, 1704, 1596, 1324\text{ cm}^{-1}$. ESI (+) LRMS (m/z): 611.03 [$\text{M} + \text{Na}$] $^+$.

tert-Butyl-(2S,3R)-4-(N-allyl-2-(hex-5-enyloxy)-4-methoxyphenylsulfonamido)-3-hydroxy-1-phenylbutan-2-ylcarbamate (11e). Title compound was obtained from **10b** and **7a**, as described for **11a** in 77% yield after flash-chromatography (3:1 hexanes:EtOAc) as a colorless oil. $[\alpha]_{\text{D}}^{20} -6.6$ (c 1.96, CHCl_3). ^1H NMR (500 MHz, CDCl_3) δ 1.36 (s, 9H), 1.60–1.66 (m, 2H), 1.87–1.97 (m, 2H), 2.13–2.17 (m, 2H), 2.91–2.98 (m, 2H), 3.27–3.39 (m, 2H), 3.79 (br s, 2H), 3.87 (s, 3H), 3.91–3.99 (m, 2H), 4.08 (t, $J = 6.7$ Hz, 2H), 4.65 (d, $J = 7.1$ Hz, 1H), 4.98 (d, $J = 10.1$, 1H), 5.04 (d, $J = 17.1$, 1H), 5.13–5.19 (m, 2H), 5.63–5.73 (m, 1H), 5.78–5.86 (m, 1H), 6.50–6.53 (m, 2H), 7.21–7.31 (m, 5H), 7.88 (d, $J = 8.7$ Hz, 1H). ^{13}C NMR (100 MHz, CDCl_3) δ 25.0, 28.3, 33.3, 35.3, 51.2, 52.2, 54.6, 55.7, 69.2, 71.8, 79.5, 100.3, 104.2, 115.1, 119.0, 119.6, 126.3, 128.4, 129.6, 133.6, 137.9, 138.2, 156.1, 157.7, 164.8. FT-IR (film, NaCl) $\nu_{\text{max}} = 3392, 2932, 1702, 1595, 1324\text{ cm}^{-1}$. ESI (+) LRMS (m/z): 611.04 [$\text{M} + \text{Na}$] $^+$.

tert-Butyl-(2S,3R)-4-(N-allyl-4-methoxy-2-(pent-4-enyloxy)phenylsulfonamido)-3-hydroxy-1-phenylbutan-2-ylcarbamate (11f). Title compound was obtained from **10b** and **7b**, as described for **11a** in 86% yield after flash-chromatography (3:1 hexanes:EtOAc) as a colorless oil. $[\alpha]_{\text{D}}^{20} -5.6$ (c 1.10, CHCl_3). ^1H NMR (400 MHz, CDCl_3) δ 1.32 (s, 9H), 1.94 (quintet, $J = 7$ Hz, 2H), 2.65 (q, $J = 7$ Hz, 2H), 2.86–2.96 (m, 2H), 3.27 (dd, $J = 7.4, 14.8$ Hz, 1H), 3.34–3.38 (m, 1H), 3.76 (br s, 2H), 3.82 (s, 3H), 3.87–3.92 (m, 2H), 4.04 (t, $J = 6.5$ Hz, 2H), 4.65 (d, $J = 8.2$ Hz, 1H), 4.98–5.15 (m, 4H), 5.57–5.63 (m, 1H), 5.75–5.86 (m, 1H), 6.46–6.49 (m, 2H), 7.12–7.27 (m, 5H), 7.83 (d, $J = 8.5$ Hz, 1H). ^{13}C NMR (100 MHz, CDCl_3) δ 27.8, 28.1, 29.7, 35.3, 51.0, 51.9, 54.5, 55.6, 68.4, 71.8, 79.3, 100.2, 104.2, 115.7, 119.0, 119.5, 126.1, 128.2, 129.5, 133.4, 137.2, 137.9, 155.9, 157.6, 164.7. FT-IR (film, NaCl) $\nu_{\text{max}} = 3390, 2976, 1710, 1597, 1325\text{ cm}^{-1}$. ESI (+) LRMS (m/z): 597.13 [$\text{M} + \text{Na}$] $^+$.

tert-Butyl-(2S,3R)-4-(N-allyl-2-(but-3-enyloxy)-4-methoxyphenylsulfonamido)-3-hydroxy-1-phenylbutan-2-ylcarbamate (11g). Title compound was obtained from **10b** and **7c**, as described for **11a** in 78% yield after flash-chromatography (3:1 hexanes:EtOAc) as a colorless oil. ^1H NMR (500 MHz, CDCl_3) δ 1.34 (s, 9H), 2.62 (q, $J = 7$ Hz, 2H), 2.88–2.96 (m, 2H), 3.27 (dd, $J = 7.8, 15.1$ Hz, 1H), 3.34–3.38 (m, 1H), 3.76 (br s, 2H), 3.85 (s, 3H), 3.87–3.99 (m, 2H), 4.10 (t, $J = 6.5$ Hz, 2H), 4.65 (br s, 1H), 5.10–5.22 (m, 4H), 5.57–5.63 (m, 1H), 5.87–5.95 (m, 1H), 6.49 (d, $J = 2.2$ Hz, 1H), 6.51 (dd, $J = 2.3, 8.7$ Hz, 1H), 7.18–7.37 (m, 5H), 7.85 (d, $J = 8.7$ Hz, 1H). ^{13}C NMR (100 MHz, CDCl_3) δ 27.8, 28.1, 35.3, 51.0, 51.9, 54.5, 55.6, 68.4, 71.8, 79.3, 100.2, 104.2, 115.7, 119.0, 119.5, 126.2, 128.2, 129.5, 133.4, 137.2, 137.9, 155.9, 157.6, 164.7. FT-IR (film, NaCl) $\nu_{\text{max}} = 3390, 2976, 1710, 1597, 1325\text{ cm}^{-1}$. ESI LRMS (m/z): 582.95 [$\text{M} + \text{Na}$] $^+$.

tert-Butyl-(2S,3R)-4-(N-allyl-2-(allyloxy)-4-methoxyphenylsulfonamido)-3-hydroxy-1-phenylbutan-2-ylcarbamate (11h). Title

compound was obtained from **10b** and **7d**, as described for **11a** in 80% yield after flash-chromatography (3:1 hexanes:EtOAc) as a colorless oil. ^1H NMR (400 MHz, CDCl_3) δ 1.33 (s, 9H), 2.83–2.96 (m, 2H), 3.25–3.36 (m, 2H), 3.77 (br s, 2H), 3.83 (s, 3H), 3.87–3.94 (m, 2H), 4.56–4.67 (m, 3H), 5.07–5.14 (m, 2H), 5.33 (d, $J = 10.5$ Hz, 1H), 5.44 (d, $J = 17.2$ Hz, 1H), 5.57–5.64 (m, 1H), 6.00–6.10 (m, 1H), 6.47 (d, $J = 1.9$ Hz, 1H), 6.51 (dd, $J = 1.9, 8.9$ Hz, 1H), 7.16–7.28 (m, 5H), 7.85 (d, $J = 8.7$ Hz, 1H). ^{13}C NMR (100 MHz, CDCl_3) δ 28.2, 35.3, 51.3, 52.1, 54.5, 55.6, 69.9, 71.8, 79.3, 100.6, 104.5, 119.0, 119.4, 119.8, 126.2, 128.2, 129.5, 131.8, 133.4, 137.9, 155.9, 157.0, 164.7. FT-IR (film, NaCl) $\nu_{\text{max}} = 3390, 2976, 1710, 1597, 1325\text{ cm}^{-1}$. ESI (+) LRMS (m/z): 569.06 [$\text{M} + \text{Na}$] $^+$.

Compound 13a. To a stirring solution of **11a** (63 mg, 0.1 mmol) in CH_2Cl_2 (2 mL) was added a solution of 30% trifluoroacetic acid in CH_2Cl_2 , and the resulting mixture was stirred for 30 min. The solvent was evaporated under reduced pressure, and the residue was dissolved in CH_3CN (2 mL). To this solution was added **12** (31 mg, 0.11 mmol), followed by $i\text{-Pr}_2\text{NEt}$. After stirring for 24 h, the reaction mixture was concentrated in vacuo and the resulting residue was subjected to flash-chromatography (1:1 hexanes:EtOAc) to give **13a** (36 mg, 53% yield) as a colorless oil. $[\alpha]_{\text{D}}^{20} -13.1$ (c 1.50, CHCl_3). ^1H NMR (500 MHz, CDCl_3) δ 1.28–1.31 (m, 6H), 1.47–1.51 (m, 3H), 1.58–1.61 (m, 3H), 1.84–1.88 (m, 2H), 1.96–1.99 (m, 2H), 2.01–2.13 (m, 2H), 2.79–2.84 (m, 1H), 2.88–2.92 (m, 1H), 3.09–3.15 (m, 1H), 3.24–3.40 (m, 3H), 3.61 (br s, 1H), 3.64–3.72 (m, 2H), 3.83–3.92 (m, 4H), 3.93–3.96 (m, 1H), 4.05 (t, $J = 6.7$ Hz, 2H), 4.90–5.03 (m, 4H), 5.64 (d, $J = 5$ Hz, 1H), 5.66–5.82 (m, 2H), 6.46 (s, 1H), 6.51 (d, $J = 8.8$ Hz, 1H), 7.17–7.26 (m, 5H), 7.83 (d, $J = 8.8$ Hz, 1H). ^{13}C NMR (125 MHz, CDCl_3) δ 27.9, 28.2, 28.1, 29.4, 31.7, 32.9, 33.1, 35.1, 45.1, 49.8, 52.1, 54.8, 55.5, 68.9, 69.3, 70.5, 72.0, 73.1, 100.1, 103.9, 109.0, 114.6, 114.9, 118.9, 126.3, 128.2, 129.1, 133.4, 137.4, 137.8, 138.0, 155.2, 157.4, 164.6. FT-IR (film, NaCl) $\nu_{\text{max}} = 3343, 2928, 1721, 1595, 1325\text{ cm}^{-1}$. ESI (+) HRMS (m/z): [$\text{M} + \text{Na}$] $^+$ calcd for $\text{C}_{36}\text{H}_{50}\text{N}_2\text{O}_9\text{S}$, 709.3135; found, 709.3136.

Compound 13b. Title compound was obtained from **11b** and **12** as described for **13a** in 55% yield after flash-chromatography (1:1 hexanes:EtOAc) as a colorless oil. ^1H NMR (500 MHz, CDCl_3) δ 1.27–1.32 (m, 3H), 1.41–1.53 (m, 3H), 1.57–1.62 (m, 1H), 1.92–1.99 (m, 4H), 2.27 (q, $J = 7.05$, 2H), 2.80 (dd, $J = 10, 14$ Hz, 1H), 2.86–2.91 (m, 1H), 3.01 (dd, $J = 4, 14$ Hz, 1H), 3.10–3.15 (m, 1H), 3.27–3.33 (m, 2H), 3.38 (dd, $J = 8.6, 15.2$ Hz, 1H), 3.61 (br s, 1H), 3.64–3.70 (m, 2H), 3.81–3.84 (m, 5H), 3.88–3.95 (m, 2H), 4.05 (t, $J = 6.6$ Hz, 2H), 4.89–5.09 (m, 5H), 5.63 (d, $J = 5.2$ Hz, 1H), 5.65–5.73 (m, 1H), 5.77–5.85 (m, 1H), 6.46 (d, $J = 2$ Hz, 1H), 6.51 (dd, $J = 2.1, 8.8$ Hz, 1H), 7.17–7.26 (m, 5H), 7.83 (d, $J = 8.8$ Hz, 1H). ^{13}C NMR (100 MHz, CDCl_3) δ 25.7, 27.9, 29.7, 33.1, 35.4, 45.1, 49.8, 52.1, 55.1, 55.7, 68.5, 69.5, 70.7, 72.2, 73.2, 100.3, 104.2, 109.2, 114.8, 115.7, 119.2, 126.4, 128.4, 129.3, 133.6, 137.1, 137.6, 138.2, 155.4, 157.5, 164.8. ESI (+) HRMS (m/z): [$\text{M} + \text{H}$] $^+$ calcd for $\text{C}_{35}\text{H}_{48}\text{N}_2\text{O}_9\text{S}$, 673.3159; found, 673.3153.

Compound 13c. Title compound was obtained from **11c** and **12** as described for **13a** in 81% yield after flash-chromatography (1:1 hexanes:EtOAc) as a colorless oil. ^1H NMR (500 MHz, CDCl_3) δ 1.31–1.35 (m, 3H), 1.50–1.54 (m, 3H), 1.62–1.67 (m, 1H), 2.00 (q, $J = 7$ Hz, 2H), 2.65 (q, $J = 6.7$ Hz, 2H), 2.82–2.87 (m, 2H), 2.91–2.94 (m, 1H), 3.06 (dd, $J = 4.1, 14.2$ Hz, 1H), 3.13–3.19 (m, 1H), 3.30–3.43 (m, 3H), 3.62 (br s, 1H), 3.68–3.74 (m, 2H), 3.85–3.88 (m, 4H), 3.92–3.99 (m, 2H), 4.13 (t, $J = 6.9$ Hz, 2H), 4.93–5.05 (m, 2H), 5.07–5.09 (m, 2H), 5.17–5.24 (m, 2H), 5.66 (d, $J = 5.1$ Hz, 1H), 5.69–5.77 (m, 1H), 5.90–5.99 (m, 1H), 6.52 (s, 1H), 6.55 (dd, $J = 2.05, 8.8$ Hz, 1H), 7.22–7.30 (m, 5H), 7.87 (d, $J = 8.8$ Hz, 1H). ^{13}C NMR (125 MHz, CDCl_3) δ 25.8, 25.9, 28.1, 29.8, 33.3, 35.6, 45.4, 50.0, 52.4, 55.2, 55.8, 68.7, 69.7, 70.8, 72.4, 73.4, 100.6, 104.5, 109.4, 114.9, 118.0, 119.5, 126.6, 128.6, 129.5, 133.5, 137.8, 138.3, 155.9, 157.6, 164.9. FT-IR (film, NaCl) $\nu_{\text{max}} = 3339, 2929, 1719,$